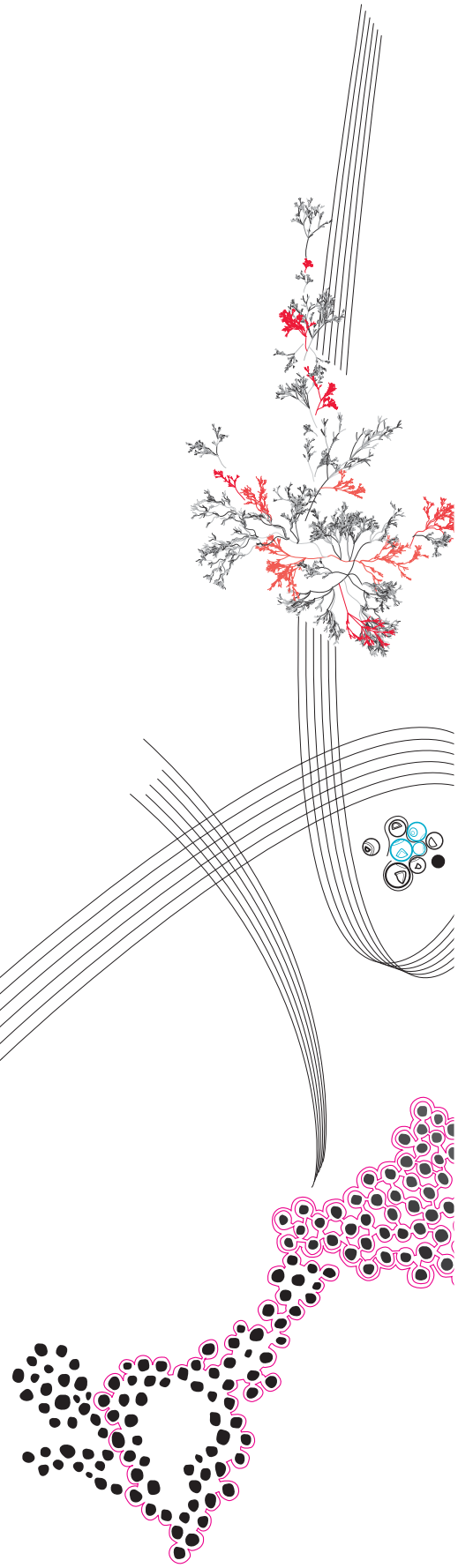

MSc Electrical Engineering
Thesis

On-demand handling system for analysis and preparation of microsamples

H.G. Sikkema

Supervisor:	Prof. Dr. Ir. M. Odijk
Daily Supervisor:	Dr. Ing. J.J.A. Lozeman
External Supervisors:	Prof. Dr. Ir. G.J.M. Krijnen
	Dr. G.S.M. Lageveen-Kammeijer

July, 2024

BIOS lab-on-a-chip group
Department of Electrical Engineering
Faculty of Electrical Engineering,
Mathematics and Computer Science,
University of Twente

UNIVERSITY OF TWENTE.

Contents

Abstract

The dynamic behaviour of hormone concentrations is crucial to our everyday life. To better understand the effects of fluctuations in this behaviour, it should be measured and studied. Current state-of-the-art minimally invasive measurement techniques can sample hormones once every 10 minutes throughout a full day. However, studies that use more invasive techniques have shown that many hormones fluctuate at shorter time scales. This research aims to bridge the gap by designing a minimally invasive hormone-sampling system with a sample rate double that of the state-of-the-art. Two novel microfluidic systems have been designed using a combination of Quake valves and optical sensors: an active droplet generator with feedback and an active injector with feedback. Combining these two microfluidic systems results in an on-demand microsample handling system. It was designed to isolate the samples and prepare them for storage and further analysis. The valves and sensors that make up the system were designed, fabricated and validated. A setup was built to control the valves according to the sensors' measurements. Using this setup, the active droplet generator with feedback was shown to work. However, due to leaks in the microfluidic chips, the droplet generator's performance could not be validated, and the injector was not tested. Despite this, both concepts have promise, and whether they can live up to that could be examined in future research.

Chapter 1

Introduction

The feeling of an upcoming deadline, an important presentation or a crucial meeting is not only an annoyance that can occupy one's mind and keep one up at night. Stress plays a vital role in our reactions and adaptation to various situations. These situations can be short-term, with a fight or flight response, but also more long-term, such as work-related stress [1]. The Hypothalamus-Pituitary-Adrenal-Axis (HPAA) is a system within the human body that handles part of these stress responses. It regulates the levels of hormones accordingly in response to these situations, known as stressors. Cortisol is one such hormone and will be the focus of this study. Fluctuations in these hormone levels signal to the rest of the body that specific actions should be taken to handle the stressors better. Deviations from the proper reactions can indicate various diseases [2]. Gaining a better understanding of how these systems function and behave normally could help us recognize any abnormal behaviour and help diagnose related diseases [3].

To study the dynamic behaviour of hormonal systems, there is a need for sampling and measurement systems that can measure the dynamic behaviour of these hormone concentrations. The hormone levels produced by the HPAA do not change gradually but vary in a much more abrupt pulsatile nature [4][5]. As such, the sampling techniques used to gather hormone samples for measurements ideally keep up with these fast changes.

Measurements can be done from various types of samples: like blood [6], sweat [7], and interstitial fluids [8]. It is also possible to measure hormone levels from urine [9] and saliva [10]; however, such measurements are not as practical when measuring cortisol changes at regular intervals over an entire day. For the other types of samples, there is a trade-off between the accuracy of the measurement and the effect of the measurement itself on hormone levels. Blood samples must be taken in a clinical setting, which might introduce extra stress and skew the results. Sweat samples are the least invasive technique as they measure on the skin. However, to measure anything, sweat is required, which needs to be stimulated in most cases, and then the measured values are orders of magnitude lower than those measured in blood [7]. Measuring hormone levels in the interstitial fluid is another approach. The cortisol is measured as it reaches the cells, so the sampled concentrations are those that affect the cells. Furthermore, it can be integrated into a wearable system that can be worn in everyday life, as demonstrated by Bhake et al. [8] with their description of the system now known as the U-Rhythm.

1.1 U-Rhythm

U-Rhythm is a sampling system developed by a group of researchers from the University of Bristol [11]. It is a minimally invasive sampling system that samples hormones in the interstitial fluid using a catheter. The system is designed to periodically sample hormones from the interstitial fluid and store them for later analysis using liquid chromatography-mass spectrometry.

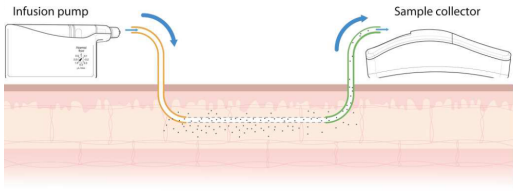

(a) The infusion pump pumps a fluid through the catheter. The catheter goes through the skin to reach the anterior abdominal wall, where it samples hormones from the interstitial fluid. The fluid is pumped into the sampler, where it is stored.

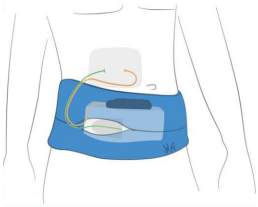

(b) Diagram showing how the system is worn like a belt around the waist.

Figure 1.1: Diagrams showing how the U-Rhythm sampler is worn. Figure reproduced from Upton et al. [12].

Figure 1.1 shows how the system is worn and connected to a catheter. An infusion pump pumps a sterile isotonic fluid through the catheter into the sampler, as shown in figure 1.1a. The catheter samples the hormones from the anterior abdominal wall. Figure 1.1b shows how the user wears the system. The whole system is worn around the waist like a belt, allowing it to sample throughout the day without impeding daily activities.

The U-Rhythm sampling system takes the continuous input flow from the catheter and periodically separates it by inserting air plugs. In figure 1.2, a schematic of the sampler is shown. The infusion pump is shown in the top left corner of the figure. It pumps the isotonic fluid through the catheter into the sampler; in this figure, the catheter is referred to as a probe. There is a pressure sensor directly behind where the probe is connected to the sampler, and this, together with the servo pump, is used to regulate the pressure in the probe to within $10mBar$. The pressure in the catheter is regulated to prevent pressure buildup as the sample store fills up. The sample stream is pushed into the sample store, and the bubble pump periodically pumps air into the sample stream, creating air plugs that physically separate the samples [8].

The system has already been used in a variety of studies to study the hormone cycles of healthy men [13][14], obese pregnant women [15] and children undergoing cardiac surgery [16]. The largest study examined the daily profile of tissue adrenal steroids from measurements of over 200 healthy volunteers [12]. These publications show how such a system can be used to further our understanding of the dynamic behaviour of hormone concentrations. Although this shows that the system is useful, there are a lot of opportunities to improve it.

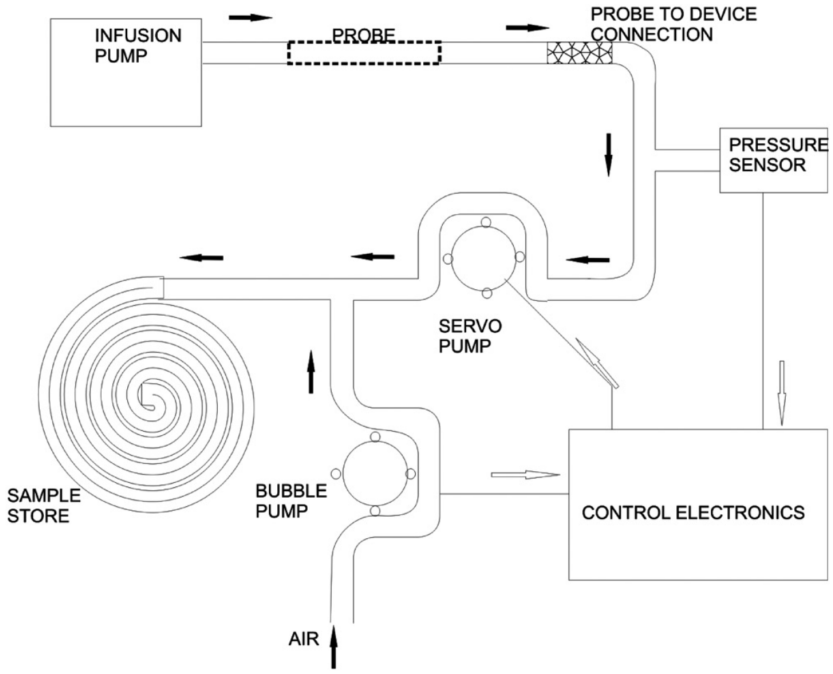

Figure 1.2: Schematic showing how the U-Rhythm sampler works, figure reproduced from Bhake et al. [8].

Various hormonal events happen at shorter time scales than the 1 sample per 10-minute sample rate of the current system [5]. Increasing the system's sample rate would allow the research to take another step toward understanding the dynamic behaviour of hormone concentrations. Due to the current approach of preparing samples for final analysis, it is difficult to increase the sampling rate. One solution could be to increase the flow rate to allow for a higher sample rate while keeping the same sample volume, which would require more total sample volume, increasing the strain on the user's body. Reducing the sample volume could be another solution, but this would make it impractical to consistently transfer them from the tubing to a well's plate, as this is currently done by hand. Neither option is ideal. Switching to a different approach to sample preparation that can handle smaller samples would allow for higher sample rates without the downsides of the current system. A sampling system that can handle smaller samples would allow for higher sampling rates without the downsides of the current system. Thus, the aim of this thesis is to develop such a system to overcome the challenges faced by the U-Rhythm.

Automating the system could allow for other benefits as well. With smaller samples, the flow rate can also be reduced, increasing the residence time of the fluid in the catheter and reducing the dispersion of the concentration before sample isolation, both of which allow the sample to be a more accurate representation of the actual hormone concentration in the body. Instead of only adding an internal standard during the sample preparation, anti-oxidants and surfactants could also be added to improve the stability of the samples, as hormones can degrade over time when stored at room temperature [17].

1.2 Goals

This study aims to design, fabricate, and test an on-demand integrated microfluidic micro-sample handling system for sample preparation and analysis that can operate at higher sample rates and with a smaller sample size than the current state-of-the-art. The system will be designed to measure cortisol levels from the interstitial fluid, but it could also be used for other applications. This goal has been subdivided into subgoals, which will be discussed in the coming chapters.

1. The first subgoal is to derive the requirements for the system. These requirements will be based on the aims of the system and the various factors influencing its performance. This subgoal will be discussed in the Theory chapter.

2. The second subgoal is to choose a design concept for the system that fits these requirements. First, the working principle of the sample isolation and preparation will be chosen. Then, this working principle will be used to define the various subcomponents, and their design concepts will be chosen. This will be discussed in the Conceptual Design chapter.

3. The third subgoal is to create a final design for the system. This starts with the design and validation of the subcomponents, followed by the final system's design. It will conclude with the design of the setup and the software with which the system will operate. This will be discussed in the Physical Design chapter.

4. The fourth and final subgoal is to test the complete system and discuss its results. Based on these results, conclusions will be drawn, and recommendations will be made for future work. This will be discussed in the Results, the Discussion and Conclusion, and the Recommendations chapters.

Chapter 2

Theory

In this chapter the aims of the micro-sample handling system will be examined in closer detail. The various physical phenomena affecting the system's behaviour will also be discussed. These will define the system requirements. To start, the improvements on the state-of-the-art will be discussed. After this, the underlying theory of the sample isolation and preparation will be addressed individually. This chapter is concluded with an overview of all the requirements that will form the basis of the conceptual design.

2.1 The overall system

The final version of the system will be part of a wearable device. Thus, it should handle the temperature changes and vibrations caused by the user's movement in different environments. It will focus on sampling cortisol concentrations over a full day. As such, where possible, the system's design choices should consider this.

Requirements:

1. The system should be designed with the end goal of sampling cortisol concentrations over a full day as part of a wearable device.

2.1.1 Sample rate

The current maximum reported sample rate of the U-Rhythm is 1 sample every 10 minutes [8]. In literature, it is reported that some hormones have a half-life below 10 minutes, which shows that a higher sampling rate could reveal more about the dynamic behaviour of hormone concentrations. The system will be designed based on a sampling rate double that of the current state of the art, so a sampling rate of 1 sample every 5 minutes.

Deviations in the sampling rate of samples could skew the results. If the sampling interval is always a few seconds longer than the expected interval, this difference would add up to a significant offset between the actual and expected measurements. As such, the average sample rate should be as close to the expected sample rate as possible. After a full day of sampling, the deviation should not add up to more than one sample period. With 288 samples per day, this results in a maximum average sample deviation of approximately $1 second$.

Requirements:

2. The system should be able to reach a sampling rate of 1 sample every 5 minutes, with a standard deviation below $1s$.

2.1.2 Sample volume

A smaller sample volume has multiple advantages. With smaller samples, the volumetric flow rate can be reduced. At lower flow rates, there is more time for hormones to diffuse through the membrane into the catheter. This allows the sample stream inside the catheter to reach higher concentrations and better represent the hormone concentrations within the body. This higher retrieval of hormones will be referred to as the recovery rate. This higher recovery rate improves the limit of detection of the entire system. Smaller droplets will allow for a smaller sample store, making the overall system smaller and more portable. The sample volume of the U-Rhythm system is mentioned to be $20\mu L$[12] at a sample rate of 1 sample per 20 minutes. With a sample rate of 1 sample every 5 minutes, this flow rate would result in samples of $5\mu L$. It was decided to use a sample volume of $1\mu L$ to benefit from all the advantages of smaller samples.

The literature about the U-Rhythm does not mention variations in the sample volume. However, the description of the assay also includes a specific approach for smaller samples, which hints at some variation in sample size. Due to the manual sample preparation used with the U-Rhythm, fluctuations in the sample size are compensated by only taking part of the sample for analysis. This method does not compensate for the change in recovery rate caused by the differences in volumetric flow rate. As this work aims to automate the sample preparation, it will no longer be possible to compensate for fluctuations in this way. Any variations in the sample volume are directly translated to an error in the measurements.

The literature regarding the U-Rhythm does not mention the error of the measured values. The studies do report extensive statistics regarding the deviations between measurements of different patients. However, the source of these deviations is unknown. It could be caused by differences between patients, U-Rhythm systems, or even differences between individual samples of one U-Rhythm system.

As there is no error margin to compare, the error margin was chosen based on the measurements shown in the literature in which the U-Rhythm was used. Upton et al.[12] measured an average cortisol concentration of $3.54nmol/L$, and the changes in the concentration that were discussed were on the order of $1nmol/L$. Based on this resolution, it was decided that the error margin should be at most half of that resolution, namely 14%.

This 14% error margin includes both the sample volume and the volume of the additives. Other factors contributing to the error are not considered for this error margin in this work. Variations in either volume will be translated directly into the final error. It is assumed that both the sample volume and the volume of additives are normally distributed, that they are independent, and that their mean values are correct. Then, the error is directly related to the standard deviation, which is simply the sum of the standard deviations of the two distributions. Dividing the error margin evenly over these two volumes results in an error margin of 7% for each volume.

Requirements:

3. The system should create samples of $1\mu L$ with an error margin of 7%.

2.1.3 Fabrication Techniques

The system will be fabricated with the rapid prototyping facilities of the BIOS lab-on-chip-group at the University of Twente. There are also extensive cleanroom facilities at the University of Twente. However, due to the training required to use either of these facilities, only one of the two was used. The fast iteration cycles that can be achieved in the rapid prototyping facilities were seen as more valuable than the precision that can be achieved in the cleanrooms.

Requirements:

4. The chip should be fabricated using the rapid prototyping facilities at BIOS.

2.2 Sample Isolation

Now that the general requirements have been defined, a closer look will be taken at the system's first task: isolate the samples. This is done to reduce the migration of hormones within the sample to the next sample. This dispersion of the sample will be referred to as crossover to prevent confusion with a specific type of dispersion that will be discussed in this section. Next to reducing this crossover, the sample isolation will also make it easier to handle individual samples. This will allow the system to feed the samples individually into the analysis equipment. To define the requirements for this part of the system, the crossover mechanisms and what can be done to reduce or prevent them will be examined closely. Before the sample isolation, the samples are inside a stream of samples. All crossover mechanisms will affect the samples in this section of the system. After sample isolation, only a smaller subset of the crossover mechanisms can still affect the samples.

2.2.1 Flow Regimes

The flow regime of the system describes how fluid travels through the system. The flow regimes are illustrated in figure 2.1. Laminar flow is the most predictable regime, while turbulent flow is unpredictable.

Fluids mix much faster in turbulent flow. Since the aim is to mix the fluid as little as possible, turbulent flow should be prevented. In laminar flow, mixing occurs only due to diffusion; this is the slowest mixing method, and thus, laminar flow is the preferable flow regime. The Reynolds number (Re), the ratio of the inertial and viscous forces inside the

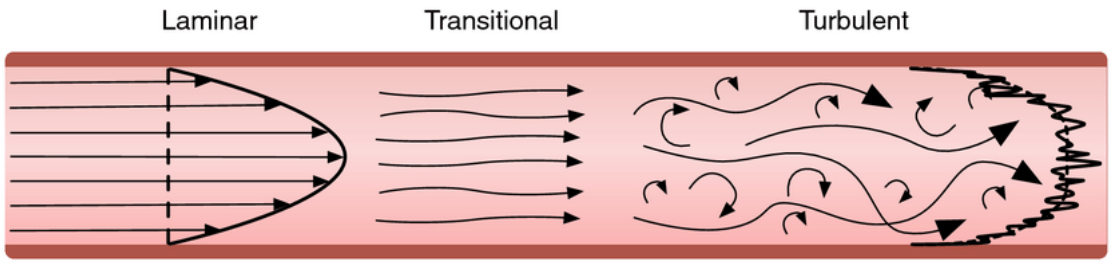

Figure 2.1: The flow regimes of fluids, laminar (left), transitional (middle) and turbulent (right). This figure is reproduced from McGurk et al.[18]

fluid, can be used to determine what flow regime the system has[19]. It can be calculated using the following equation 2.1.

$$Re = \frac{\rho u L}{\eta} \tag{2.1}$$

The Reynolds number depends on the density of the fluid (ρ), the mean flow speed of the fluid (u), the characteristic length of the channel (L) and the dynamic viscosity of the fluid (η). The viscous forces dominate at low Reynolds numbers, resulting in a laminar flow. At higher Reynolds numbers, the inertial forces dominate, and the flow becomes turbulent. There is no clear boundary between laminar and turbulent flow. It transitions gradually between Reynolds numbers of 2000 and 3000. The mean flow speed and the characteristic length can be controlled to control the Reynolds number. By choosing the channel dimensions and flow conditions, laminar flow can be created. As such, the system should fulfil the following requirement:

Requirements:

5. The channel dimensions and mean flow speed should be chosen such that the Reynolds number is below 2000 and the flow is laminar.

2.2.2 Mass Transport

The hormones in the samples move through the channel by diffusion and convection. When samples are transported by convection, they move in the flow direction without spreading. When the samples are transported by diffusion, the hormones move in all directions and are dispersed over the channel. As such, convection is preferable since this reduces the spreading of the hormones and, thus, the crossover between samples. The Péclet number (Pe) is the ratio between these two transport phenomena and can be used to determine which transport phenomenon is dominant[19]. It can be calculated using equation2.2:

$$Pe = \frac{uL}{D} \tag{2.2}$$

The Péclet number depends on the mean flow speed of the fluid (u), the characteristic length of the channel (L) and the diffusion coefficient of the hormone. Convection and diffusion are significant when the Péclet number is close to one. When the Péclet number goes to zero, diffusion dominates, and when it goes to infinity, the convection dominates. So from this, it could be concluded that the Péclet number should be made as large as possible to reduce sample crossover. However, comparing equations 2.1 and 2.2 shows that when the Péclet number increases, the Reynolds number also increases, which could lead to turbulent flow. Thus, diffusion will become a significant aspect of mass transport and should be considered.

2.2.3 Diffusion and Taylor dispersion

The diffusion rate of the sample within the channel depends on the concentration gradient. Since the system aims to measure changes in hormone concentrations over time, these concentration gradients ($\frac{\partial C}{\partial t}$) will be present in the system. The rate at which the hormone concentration changes due to diffusion can be calculated using Fick's second law, shown in equation 2.3.

$$\frac{\partial C}{\partial t} = D\frac{\partial^2 C}{\partial x^2} \tag{2.3}$$

The change in concentration over time is dependent on the diffusion coefficient (D) and the second derivative of the concentration with respect to distance ($\frac{\partial^2 C}{\partial x^2}$). In this equation, the diffusion is only considered in one dimension, which is enough for an estimation of the dispersion of the sample. In actuality, the diffusion occurs isotropically. Diffusion is a slow process. However, since the system aims to sample for 24 hours or longer, there is enough time for the hormones within the samples to crossover into other samples. In figure 2.2, the dispersion of the concentration profile caused by the diffusion over time can be seen. At $t = 0$, the system starts with a concentration pulse of which the integral equals 1; this concentration is spread further apart as time progresses. The diffusion coefficient of cortisol was calculated by Gordic et al.[20].

The concentration is spread over a few centimetres of the one-dimensional channel. This spread assumes that there is no flow inside the channel. When there is flow inside the channel, the spreading of samples is sped up significantly. Adding pressure-driven flow to the system results in Taylor dispersion, where the combination of a flow profile and diffusion results in a much more significant sample dispersion as depicted in figure 2.3. The original solute is spread out over the channel by the parabolic shape of the flow profile. The fluid in the centre of the channel flows much faster than the fluid near the channel surface. These flows drag the solute along and spread it out over the channel. This combination of the spreading through the flow profile and the diffusion spreads the sample much further than with only diffusion.

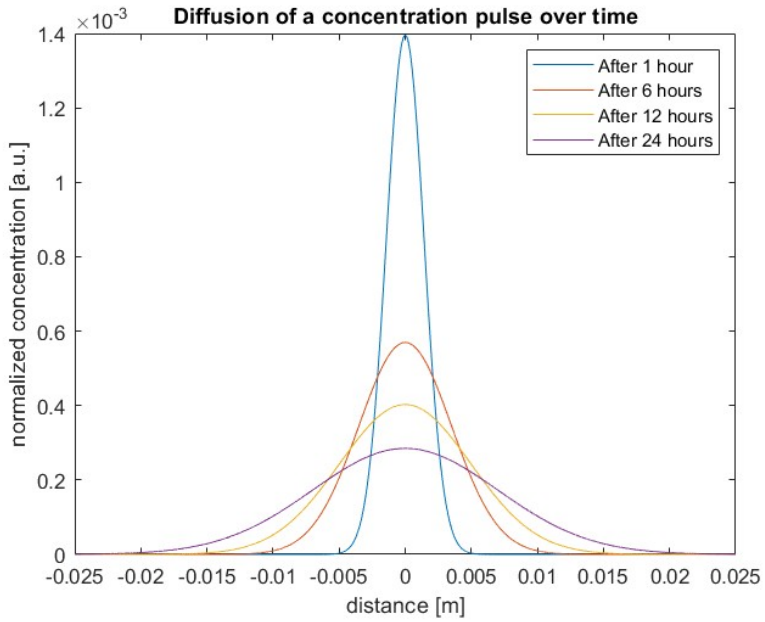

Figure 2.2: Concentration profile of a single cortisol pulse through diffusion over time.

The effect of Taylor dispersion can be calculated by replacing the diffusion coefficient in equation 2.3 with the dispersion coefficient (k)[21]. The dispersion coefficient can be calculated using equation 2.4.

$$k = \frac{r^2 u^2}{48D} \tag{2.4}$$

The dispersion coefficient depends on the radius of the channel (r), the mean flow speed of the fluid (u) and the diffusion coefficient (D). Solving equation 2.3 with this dispersion coefficient results in an equation that shows the concentration profile after a certain time. In figure 2.4, the concentration profiles can be seen when Taylor dispersion is also considered. The profiles are calculated from the same starting pulse as in figure 2.2. The dispersion coefficient is calculated using the catheter dimensions used with the U-Rhythm [22], and the mean flow speed is derived from a volumetric flow rate of $1\mu L/5min$. In figure 2.4, it can be seen that the pulses are dispersed further than with only the diffusion. Using the dimensions of the catheter tubing and a sample volume of $1\mu L$, it can be derived over how many samples the concentration pulse is dispersed. Each $1\mu L$ sample has a length of $8.8mm$, and the threshold is 5% of the maximum concentration of that curve. When considering the fluid flow with Taylor dispersion, the concentration pulse was spread over 4 samples with only diffusion and over 22 samples. The maximum sample concentration after $24hours$.

Without measures to reduce the dispersion of the hormones, the sample concentrations will slowly spread out over the sample stream. The diluted samples reaching the measurement equipment will have much lower concentrations, as shown in figure 2.4, possibly below the limit of detection of the measurement equipment. The main measure to reduce crossover

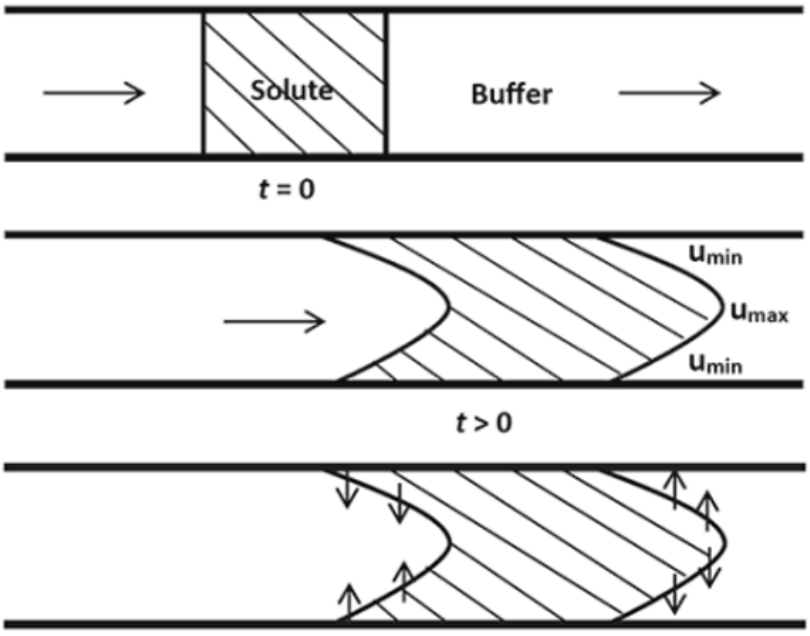

Figure 2.3: Visual representation of Taylor dispersion. The channel starts with a plug of solute stored in a buffer at t=0 (top). As the flow starts, the solute is spread according to the flow profile in the channel (middle), from where it diffuses into the buffer (bottom). Figure reproduced from a Malvern Instruments Limited white paper [21].

is the sample isolation itself, and this should prevent the crossover of hormones through diffusion. The crossover between samples before the sample isolation should be minimised by designing the system so that the flow conditions cause little diffusion. This will be done by focusing on the following requirements.

Requirements:

6. The sample isolation should prevent the crossover of hormones by diffusion between samples.
7. The stage before the sample isolation should be as short as possible to reduce Taylor dispersion.
8. The stage before the sample isolation should have an optimised flow rate to minimise the effect of Taylor dispersion.
9. The entire system should minimize dead volume to reduce the crossover between the leftover sample and the next sample.

2.2.4 Crossover through channel surfaces

The crossover between hormone samples can have multiple causes. Diffusion and Taylor dispersion are caused by hormones travelling through the fluid to reach another sample.

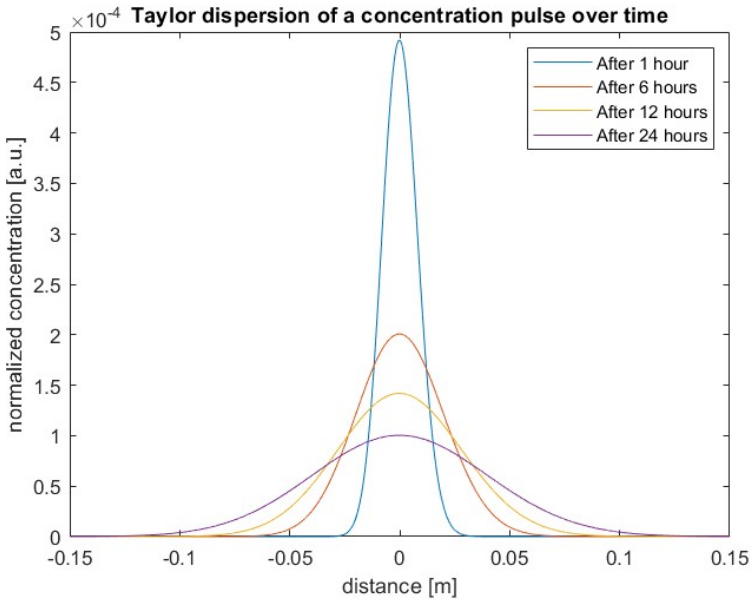

Figure 2.4: The change in the concentration profile of a single cortisol pulse through Taylor dispersion over time at a flow speed of $1\mu L/5min$.

Hormones can also crossover into or onto the surfaces of the channels and again cross over into another sample. These effects are known as sorption when the molecules attach to (adsorption) or migrate into (absorption) the material, and desorption, when they are released back into the fluid. The channel material should be chosen to reduce this type of crossover.

Requirements:

10. Adsorption and absorption should be considered in the material choice.

2.3 Sample Preparation

Automating the sample preparation will allow the system to use much smaller sample volumes, as they no longer require manual handling. These smaller samples have various advantages in terms of crossover and reduce the dilution of the samples. Placing the sample preparation on the sampler will also allow various additives to be added, which can improve the stability of the sample. These will first be discussed to understand better why the sample should be prepared. Based on that discussion, the additional requirements for sample preparation will be defined.

2.3.1 Additives

The compounds that would be interesting to add can be split into three categories: antioxidants, surfactants, and internal standards. Anti-oxidants can help reduce the degradation

of some hormones. Whether they should be added depends on the hormones of interest [23]. Surfactants can help stabilize droplets and prevent them from coalescing into fewer larger droplets [24]. The final category is the internal standards. These are essential for measuring the hormone concentration. The hormone concentrations in the samples will be measured using mass spectrometry. The various compounds in the sample will first be separated using either liquid chromatography or capillary electrophoresis. Adding an internal standard to the sample adds a reference point to the measurement results. The mass spectrum and the concentration of the internal standard are known and can be used to derive the concentrations of the hormones in the sample [25].

The internal standard concentration and total additive volume must be consistent. Variations directly translate to an error in the final measurement. As mentioned in section 2.1.1, the added volume has an error margin of 7%. As for the volume itself, it was decided to use a volume of $1\mu L$.

Requirements:

11. The sample preparation should add consistent volumes of $1\mu L$ of additives to each droplet, with an error margin of 7%.

2.4 Requirements

Below is a complete overview of the requirements. They have been organized into three categories. The first category is the design context, which contains requirements related to both the system's final goal and the available equipment. The second category contains exact technical specifications for the volumes and the sample rate. The third and final category contains requirements regarding the temporal resolution of the system. The temporal resolution is a crucial aspect of the system. As such, it has its own category within the requirements. The numbering of the requirements has been redone according to the three categories.

Requirements:

1. Design context:
   (a) The system should be designed with the end goal of sampling cortisol concentrations over time over a full day as part of a wearable device. (section 2.1)
   (b) The chip should be fabricated using the rapid prototyping facilities at BIOS. (section 2.1.3)
   (c) The sample isolation should prevent the crossover of hormones by diffusion between samples. (section 2.2.3)
   (d) Adsorption and absorption should be considered in the material choice. (section 2.2.4)
2. Technical Specifications:
   (a) The system should be able to reach a sampling rate of 1 sample every 5 minutes, with a standard deviation below $1s$. (section 2.1.1)
   (b) The system should create samples of $1\mu L$ with an error margin of 7%. (section 2.1.2)
   (c) The sample preparation should add consistent volumes of $1\mu L$ of additives to each droplet, with an error margin of 7%. (section 2.3.1)

   Within the specifications, the temporal resolution of the system has an essential role, as such it has its' own category.
3. Temporal Resolution:
   (a) The channel dimensions and mean flow speed should be chosen such that the Reynolds number is below 2000 and the flow is laminar. (section 2.2.1)
   (b) The stage before the sample isolation should be as short as possible to reduce Taylor dispersion. (section 2.2.3)
   (c) The stage before the sample isolation should have an optimised flow rate to minimise the effect of Taylor dispersion. (section 2.2.3)
   (d) The entire system should minimize dead volume to reduce the crossover between the leftover sample and the next sample. (section 2.2.3)

Chapter 3

Conceptual Design

The aim of this chapter is to determine a design concept that fits the requirements defined in chapter 2. The design concept is split into components, and these are discussed individually. The designs of the components were chosen based on the requirements, related theory, and state-of-the-art.

3.1 Design Concept

Currently, our system can be described according to the block diagram in figure 3.1. The system starts with an incoming sample stream. The individual samples are isolated and prepared for storage and analysis before being sent towards the sample storage. The system will be designed as an integrated microfluidic system due to the emphasis of the requirements on keeping the system length scales small and the system portable. Droplet generators will be discussed for the sample isolation, as these are a common microfluidic solution for isolating individual samples. For the sample preparation, a closer look will be taken at microfluidic injectors.

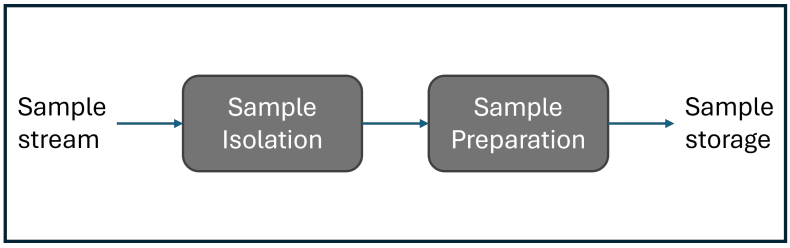

Figure 3.1: Block diagram of the system thus far.

3.1.1 Droplet Generators

In microfluidics, droplet generators are often used to retain temporal resolution by isolating samples, thus preventing diffusion. In this work, droplet generators will be used to fulfil requirement 1c. These droplets can be used to study individual cells or as microreactors to study chemical reactions[26]. The fluid of which the droplets are made, and the fluid in which the droplets are suspended should be immiscible. In this system, the droplet will be made of the aqueous sample stream. For the continuous phase between the droplets, either an oil or a gas could work. Requirement 1a specifies that the system should be designed for cortisol sampling, and cortisol is a non-polar molecule that might diffuse into the oil.

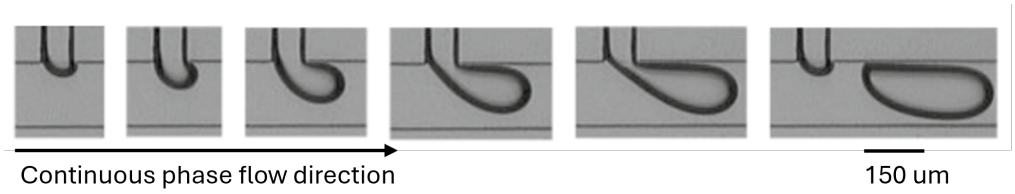

Figure 3.2: Example of a droplet created in a T-junction passive droplet generator. The continuous phase flows from left to right and the dispersed phase flows from the top into the channel. The figure is adapted from Liu et al. [27].

As such, the droplets will be made of water and surrounded by gas.

There are various types of droplet generators. The designs can be split into two categories: active and passive droplet generators. The distinction is based on whether an outside force actively controls the droplet's creation. If this is not the case, it is called a passive droplet generator. In a passive droplet generator, multiple constant fluid flows meet at a junction. Due to fluid instabilities, droplets start breaking off from one of the streams. An example of the passive droplet generation is shown in figure 3.2. The surface properties of the channels determine Which fluid becomes the droplet (the dispersed phase) and which fluid becomes the medium surrounding the droplets (the continuous phase). For example, a hydrophobic channel will have hydrophilic droplets. The droplet size and frequency depend on a complex balance of surface properties, fluid properties, flow rates, and pressures. Any fluctuations will cause the balance to shift and will result in different droplet sizes and frequencies[26]. This is without considering the added complexity of stabilizing a segmented flow using both compressible and in-compressible liquids[28]. With a passive droplet generator, it will be impossible to meet the requirements under category 2 and requirement 1a. The strict requirements for deviations in sample volume and sample rate require a very tight balance of surface properties, fluid properties, flow rates, and pressures. This can not be guaranteed when the system is worn and experiences both vibrations due to the movement of the user and temperature changes due to changes in the environment.

Our system requires an active droplet generator, a more robust approach to droplet generation. In such generators, an outside force actively controls the droplet creation. For example, one active droplet generator design uses electrowetting to create droplets [29]. Applying voltage to a surface can alter the wetting of the surface so that droplets can be moved around across electrodes. The droplets can be pulled apart and merged, as shown in figure 3.3a. The droplets can be moved around and combined with other droplets by placing the electrodes in a grid[30], as shown in figure 3.3b. With these two together, the droplets could be isolated and prepared.

This design is not ideal for this work as the wettability of the channel surface can change due to water and air [31], affecting the resulting droplets. Whether this would work well in a portable device is also uncertain, as changes in the direction of gravity and vibrations might affect the droplet size. Another active droplet generator design uses valves to control one of the input flows [32]. The droplet volume is controlled by controlling the time the valve is open. This feedforward control requires precise knowledge of the flow conditions to create droplets with a consistent volume, as shown in figure 3.4. The flow conditions in this work are inconsistent since the sample store will fill up over time, and the pressure

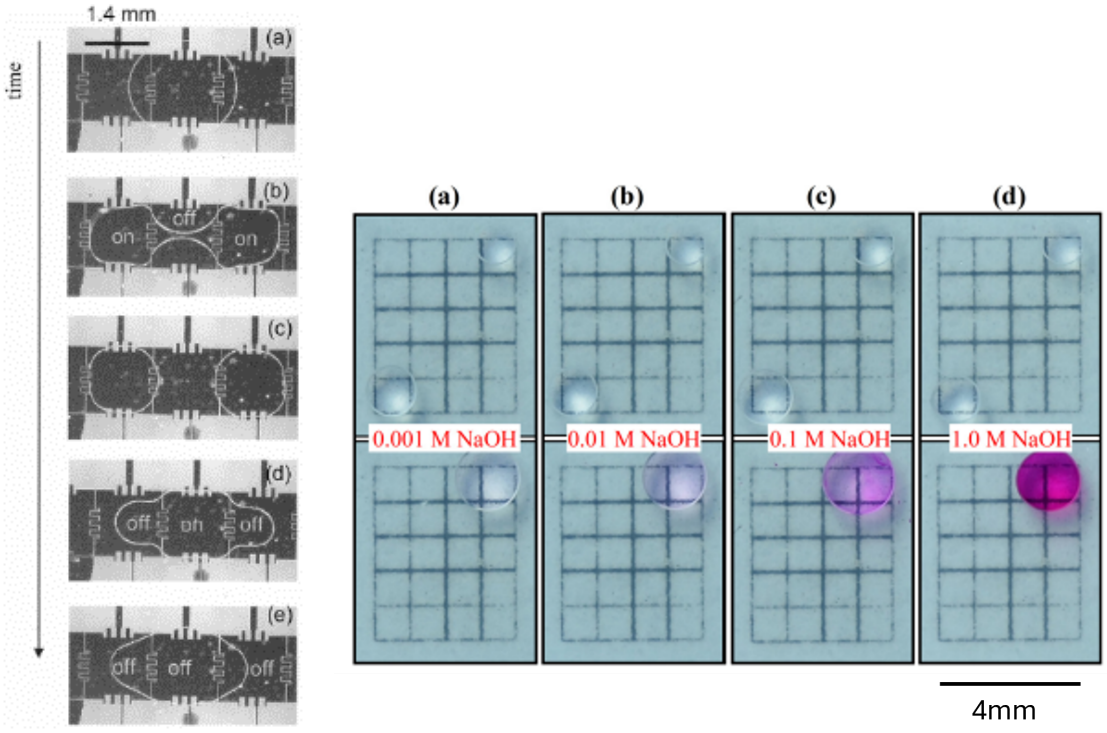

(a) (b)

Figure 3.3: Examples of electrowetting for sample isolation and preparation. A) The splitting and merging of droplets using electrowetting. Droplets can also be created using this method. This figure is reproduced from Cho et al. [29] B) Droplet manipulation using an electrowetting platform. This figure is adapted from Cao et al. [30].

needed to create the right flow speeds will increase. However, if the system is aware of the actual flow conditions using feedback instead of feedforward, the valve-controlled flow might be able to create consistent droplets. It was decided to take inspiration from this approach[32] and use valves to control the flow, together with a sensor to measure the size of the droplet, which would function as a feedback system to create droplets of the right size. By also adding a valve into the flow of the dispersed phase, total control over the system is given, and any unwanted droplet breakup is prevented.

Before continuing, a nuance in the terminology regarding droplet generators will be explained. So far, droplet generators have been discussed for making droplets. However, they are referred to differently depending on their size relative to the channel. In figure 3.3, there are clear examples of what is referred to as droplets. In figure 3.4 are examples of plugs. This work will continue with plugs. As plugs cannot pass by one another, they allow for the sequential storage of samples without any chance for the order to change. The system used to create these plugs is still called a droplet generator.

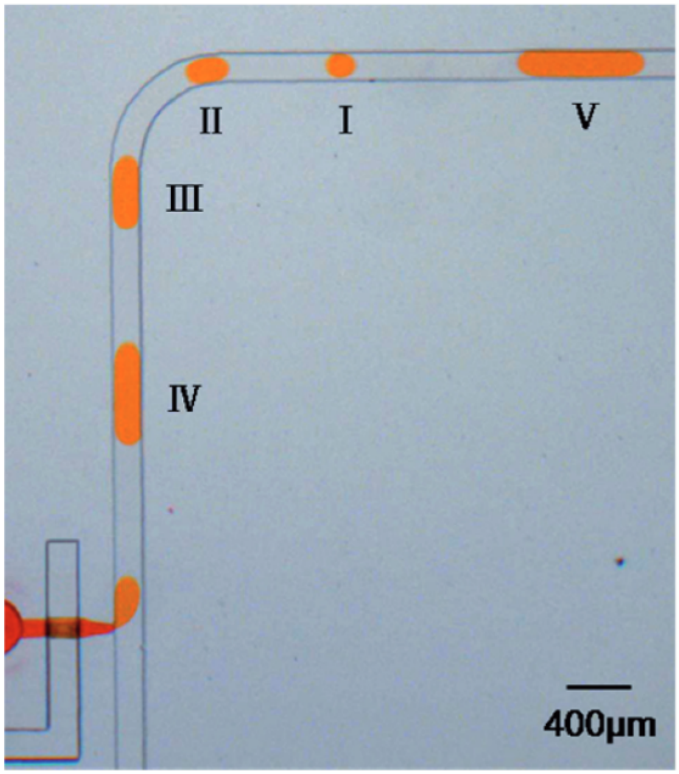

Figure 3.4: Active droplet generator using valve actuation to control the droplet size. Figure reproduced from Zeng et al.[32]

3.1.2 Active Droplet Generator with Feedback

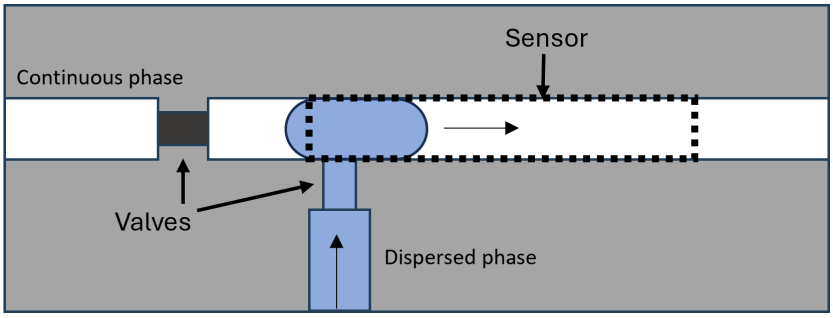

Figure 3.5: Basic concept of the active droplet generator with feedback.

Figure 3.5 shows the basic concept of this active droplet generator with feedback. It is a T-junction style droplet generator similar to figure 3.4. Two flows come together in this T-junction. By opening one valve at a time, the fluid that enters the junction can be chosen. When the sensor detects that the plug is large enough, the plug can be sent along, and the next plug can be made. It has three parts that still need to be designed: the valve, the sensor, and the control system, which ties the whole system together.

A camera could be used as a sensor, and with some image processing, the volume of the plug could be measured. Fast volume measurements are crucial for the droplet generator's response time. This would require a computer that constantly processes images. This is computationally complex and would require a camera and a computer. Carrying around

a computer capable of image processing in a device intended to be portable is non-ideal. The entire system would also require a large battery to be able to keep sampling for a full day. This would not fit well with requirement 1a, and the system would become expensive due to all that equipment. Since the dimensions of the channel are known, it is known how far into the channel the plug should extend when it is exactly $1\mu L$. At this point along the channel, a single light sensor could also measure when the plug is the correct size. The readout of such a sensor could be done with a small amplifier circuit and an analogue pin of a microcontroller. This approach fulfils requirement 1a and would be cheaper.

The operation of the droplet generator is shown in figure 3.6. It shows the creation of the plug from the start. The sensor detects the sample when the plug reaches the correct volume. Then, the system closes the valve to the dispersed phase and opens the valve to the continuous phase.

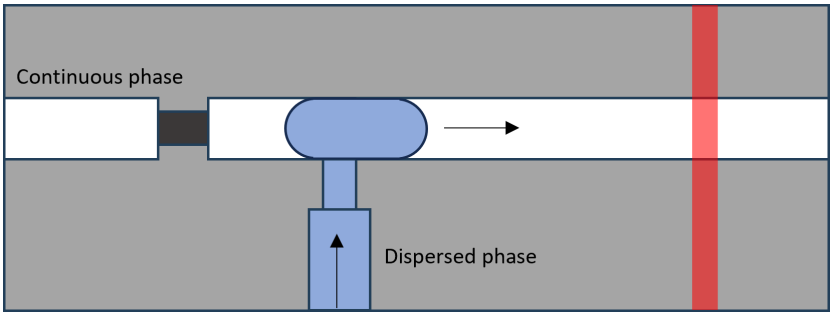

(a) Step 1: the plug creation begins.

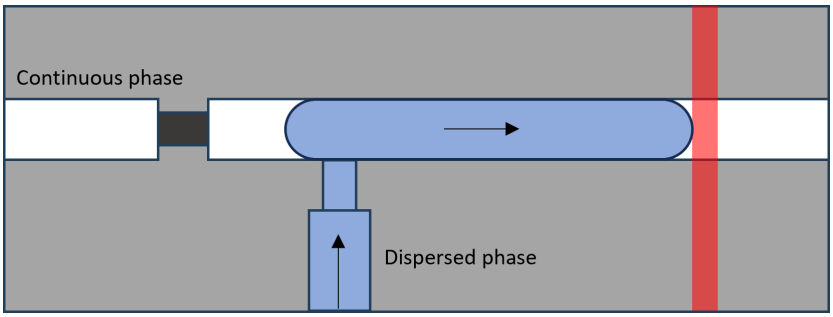

(b) Step 2: the plug creation is finished.

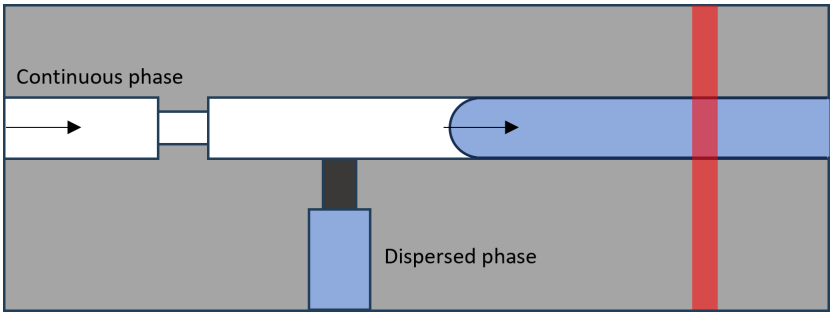

(c) Step 3: the plug is pushed along the channel.

Figure 3.6: Schematic drawings showing how the active droplet generator with feedback would create droplets. a) The plug creation starts, and the flow with the dispersed phase is allowed into the channel. b) Once the plug reaches the sensor (red line), the flow with the dispersed phase will be turned off. c) Once the dispersed flow is turned off, the continuous flow is turned on, and the plug is pushed along.

3.1.3 Active Injector with Feedback

An injector is a device that injects a volume into an existing droplet. An example can be seen in figure 3.7. This picoinjector[33] injects small volumes of additives into the droplets when the electric field is on; switching the electric field allows the droplets to be injected selectively. Unfortunately, this design does not meet the requirements. The volume of the additives is 6 orders of magnitude too small, and the injected volumes tend to vary with $\pm 50\%$.

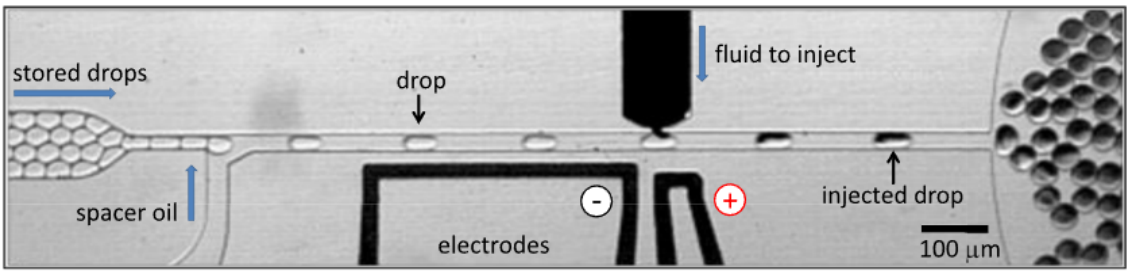

Figure 3.7: A high throughput picoinjector, the injection can be controlled with the electric field between the electrodes. The figure is reproduced from Abate et al. [33].

The picoinjector[33] can be used to understand what is needed to form an injector. In this work, the injector should inject the same volume of additives into each plug; as such, the injector needs a mechanism to ensure that each droplet receives an injection and that the injected volume fits requirement 2c. During the plug creation in the sample isolation stage, the droplet's location is known and stationary, as shown in figure 3.6b. Since the plug volume, the additive volume, and the channel dimensions are known, how far the combination of the two volumes extends into the channel is also known. By placing a sensor at this point in the channel, it can be measured when enough additive volume has been added. So, the components needed for the droplet generator can also be used for the injector. Since the requirement for the sample volume is identical to that of the additive volume, requirements 2b and 2c, the same principle should be able to fulfil both requirements. In figure 3.8, the injector operation can be seen. It starts after step 2 of the sample isolation operation, shown in figure 3.6b. The additives are injected directly into the plug until it reaches a total size of $2\mu L$, shown in figures 3.8a and 3.8b. The second sensor should measure this and signal to the system that the plug can be sent along as shown in figure 3.8c.

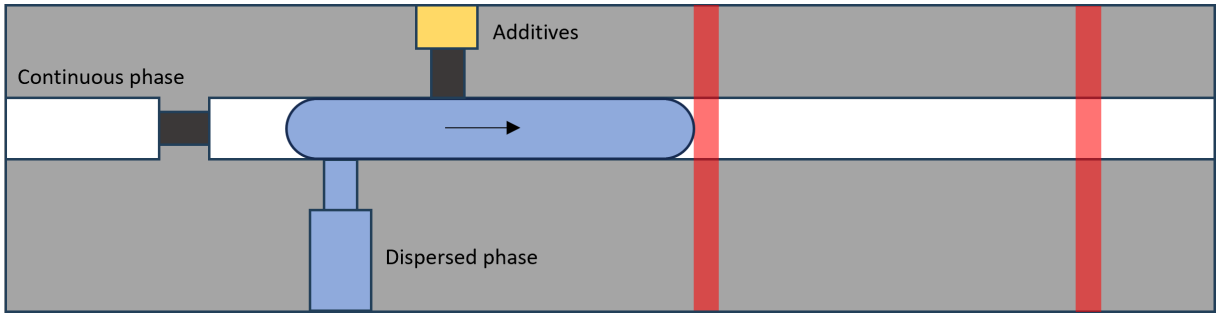

(a) Step 1: the additive injection begins

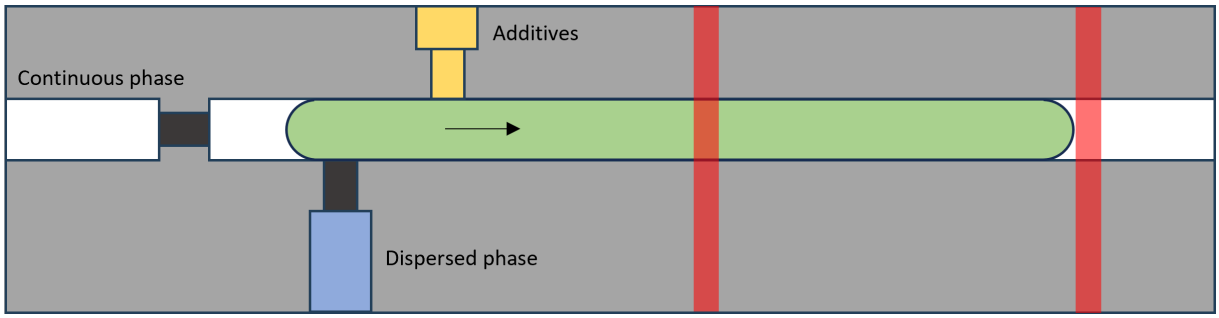

(b) Step 2: the additive injection is finished.

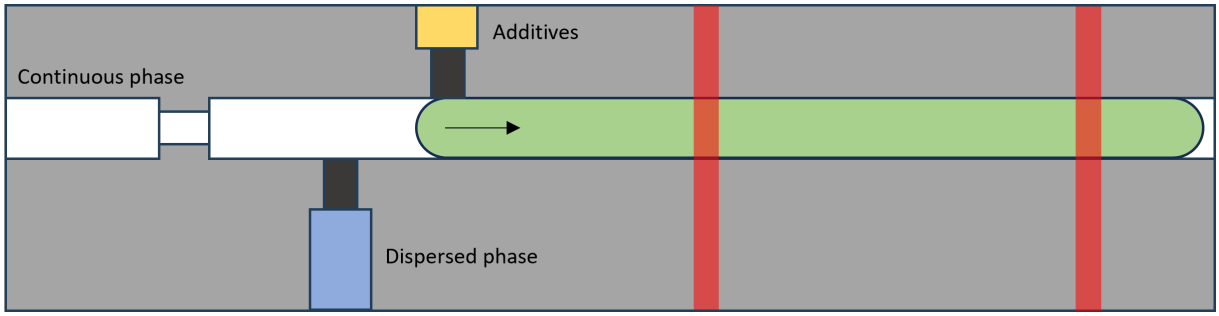

(c) Step 3: the plug is pushed along the channel.

Figure 3.8: Schematic drawings showing how the injector would inject a volume of additives in plugs. a) The additive injection starts, and the flow with the additives is allowed into the channel. b) Once the plug reaches the second sensor (right red line), the flow with the additives will be turned off. c) Once the additive flow is turned off, the continuous flow is turned on, and the plug is pushed along.

3.2 Components

As discussed in section 3.1.2, for the droplet generator to work there are still three components that need to be designed. In this section, the valve, the sensor, and the setup designs will be chosen based on the requirements.

3.2.1 Valve

The valve design is based on a push-up quake valve design[34]. The valves are designed to be used on-chip, require no clean-room facilities to produce, and have been shown to be reliable. Since the valves can be made on-chip, the channel length between the valves and the T-junction can be kept short, fulfilling both requirements 3b and 3d. The valves have already been produced with the BIOS rapid prototyping facilities before, fulfilling requirement 1b[34]. The push-down quake valve has a similar design that fulfils most of the requirements. However, it is a less robust valve[35]. In appendix A, a COMSOL simulation shows that certain valve parts are under much more stress, which could explain the lower robustness of the push-down quake valve.

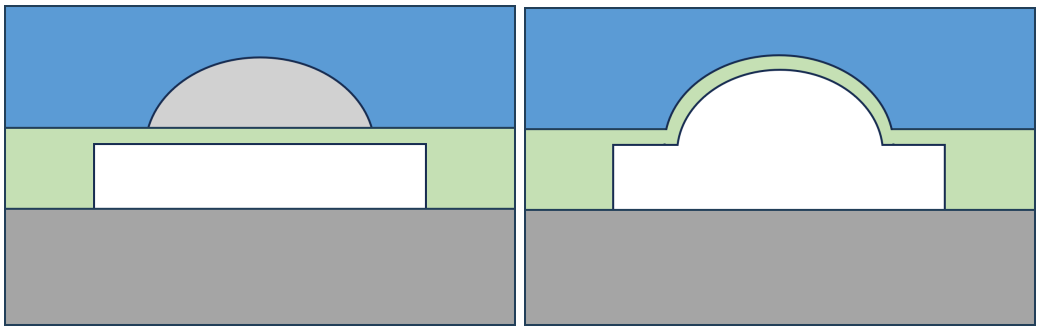

Figure 3.9: Schematic of the push-up quake valve design. the valve consists of 3 layers. The top layer (blue) contains the flow channel through which the fluid flows. The middle layer (green) contains the control channel used to actuate the valve. The bottom layer (grey) is the substrate, which is there to close the control channel and for structural support. The control layer is made of a flexible material and will be pushed into the flow channel when the valve is closed. The open state can be seen on the left with a light grey fluid in the flow channel. The closed state can be seen on the right.

The push-up quake valve can be seen in figure 3.9. It closes by pushing the flexible middle layer, the control layer, into the flow channel above. This is done by applying enough pressure on the control channel. The exact dimensions and material will be discussed in chapter 4.

3.2.2 Sensor

The sensor should be able to measure the difference between the gaseous continuous phase and the aqueous segmented phase to determine when the plug reaches the correct size. In section 3.1.2, it was mentioned that a light sensor could be a good choice. Another approach would be an electrical sensor that would measure the resistance or permittivity of the channel. However, this would complicate the fabrication process, and it would not fit requirement 1b as the fabrication of electrodes requires clean room processes.

The sensor needs to measure the difference in an optical property of water and gas to measure the difference between them. The attenuation of light through water and air is not equal. However, the difference in attenuation at the distances involved in the microfluidic device is negligible. The refractive index difference between water ($n = 1.33$) and air ($n = 1$ is much more significant. There are two approaches to measure this difference in refractive index. The top of the channel can be used as a mirror, or the shape of the channel can be used as a lens.

Using the top of the channel as a mirror would require very accurate alignment of the sensor and the photodiode, and the top surface of the chip would also require fabrication at an angle to prevent total internal reflection. Using the channel as a lens is an easier approach. Snell's law is used to understand this approach. This law describes the change in the angle of incidence of light at the interface of two materials in relation to their refractive indices. The law can be seen in equation 3.1.

$$\frac{\sin\theta_1}{\sin\theta_1} = \frac{n_2}{n_1} \tag{3.1}$$

Snell's law describes how the angles of incidence (θ_1 & θ_2) depend on the ratio of the refractive indices (n_1 & n_2). The closer the two refractive indices are to each other, the less the angle changes. The refractive index of water (1.33) is much closer to that of materials such as glass (1.52) or PDMS(1.44)[36]. As such, when light crosses an interface from one of those materials to water or vice versa, it barely refracts. This same interface but with air instead of water would refract the light significantly more.

There are two methods to use this, shown in figure 3.10: either the channel focuses the light onto the sensor, like a lens, or refracts it away from the sensor. The first method requires the light to hit the convex side of a smooth channel at a precise distance from the sensor to focus the light onto the sensor. The second method requires the light to hit the channel on the concave side, and distance is less crucial. As such, the second method was chosen as this is more robust. The exact choice of components and the accompanying amplifier circuit are discussed in chapter 4.

3.2.3 Set up

In order to actuate the valves and read out the sensors, a larger setup is needed. The first part is the pump that makes the fluid flow. There are two types of pumps: a pressure pump and a flow pump. A pressure pump allows the user to set the pressure, and it regulates the flow rate to keep this pressure. A flow pump allows the user to set the flow rate, and it regulates the pressure to keep this flow rate. If a valve closes in front of a flow pump, the flow pump will try to push through the valve, which could damage the valve. As such, the system needs a pressure pump for the flow.

To actuate the valves, a fast switching system is needed that can either put pressure on them or not. A solenoid valve system will be used for this. This system has a pressure input and can control which outlets are set to this same pressure. By connecting this pressure outlet to the valves, the valves can be switched as well.

A data acquisition device will be needed to read out the sensor signal. This device will convert the analogue signal into a digital signal.

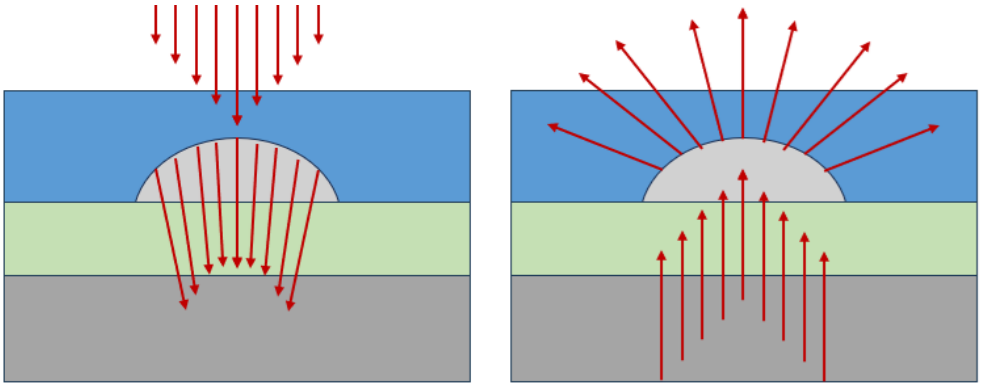

Figure 3.10: Diagrams showing the two sensor concepts using the difference in refractive index. In these diagrams, the light refracts like the channel is filled with air. If it were filled with water, the light would refract less. The arrows' directions indicate the direction of the light.

Finally, the system will need a controller that can use the measured values from the sensor to actuate the valves at the right time. A computer is the easiest choice since all other components must be connected to this controller. This computer will run a code that reads out the sensors and controls the valves.

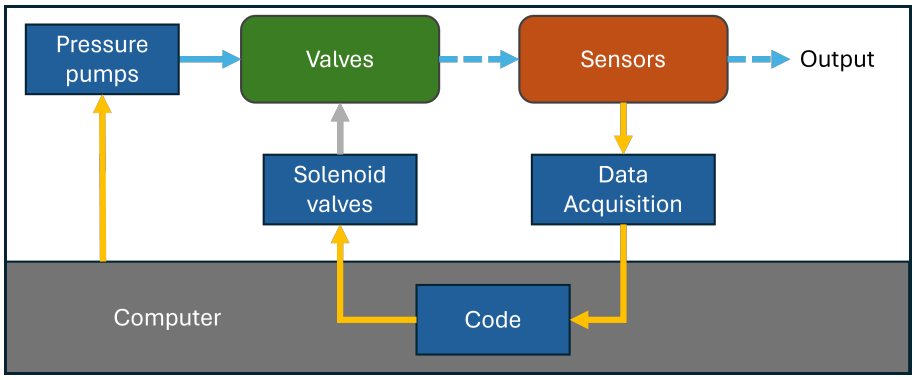

Figure 3.11: Block diagram showing how the various components of the system interact with each other. The fluids are pumped from left to right. Their flows are controlled by the valves based on the sensors' measurements.

Figure 3.11 shows a block diagram of the setup. The pressure pump pumps fluid through the system, the valves control the flow, and the sensors measure the plug size. The computer controls the whole system. It receives the sensor data from the microcontroller and actuates the solenoid valves that control the push-up quake valves on the chip accordingly. The pressure of the pressure pump and the computer control the entire system and dictate the flow conditions. These will need to be designed such that our system fulfils requirements 2a, 2b, 2c, 3a and 3c. The exact choice of equipment and the functioning of the code will be discussed in chapter 4.

Chapter 4

Physical Design

In this chapter, the design concepts from chapter 3 will be worked out into the final designs of the components and the complete system. This includes the valves, the sensors and the surrounding setup. To understand how the setup will pump the fluids and actuate the valves, a model is made to gain insight into the effects of the flow conditions on the sample dispersion.

4.1 Valves

In chapter 3, it was decided to use push-up quake valves. This section will discuss the choice of material, fabrication and exact dimensions.

4.1.1 Valve Materials

As discussed in section 3.2.1, the valve consists of 3 layers: the top layer contains the flow channel, the middle layer contains the control channel and the bottom acts as the substrate. The middle layer needs to be flexible in order for the valve to close, and all layers need to be transparent to red visible light for the sensor to work. The layers should bond well with each other, meaning that the bond should be able to withstand the pressures required for hydraulic actuation and fluid flow, and the materials should be compatible with the fabrication methods used in the rapid prototyping facilities at BIOS.

For the material of the flexible layer, 2 polymers were considered: polydimethylsiloxane (PDMS) and Flexdym. PDMS is a classic microfluidic material and has been used for this valve design in literature before[34]. It is flexible and transparent and can be made at BIOS. BIOS also has extensive experience using the material for microfluidics. The downside of PDMS is that it is permeable to small molecules such as hormones[37].

Flexdym is a novel material specialised for microfluidics, and it is positioned as the replacement of PDMS[38]. It is a type of Styrene-Ethylene-Butylene-Styrene (SEBS). It is flexible and transparent and films of SEBS can be processed into specific shapes by hot embossing at BIOS. Unlike PDMS, it has lower sorption properties, and its production can more easily be scaled up [38] as it is compatible with injection molding. Flexdym fulfils requirement 1d better than PDMS because of its' low sorption. Because of this, it was decided to test Flexdym to see if it would be possible to make valves out of it. During these tests, it became clear that fabricating chips out of Flexdym is more complicated than with PDMS. Flexdym deformed significantly during its fabrication, and bonding Flexdym

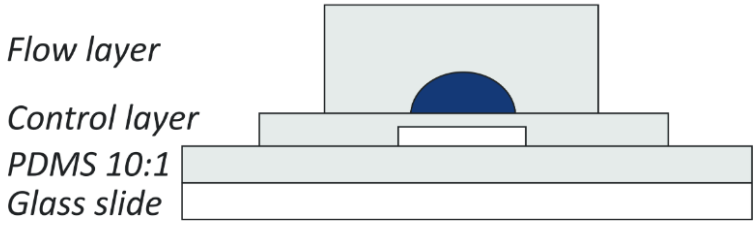

Figure 4.1: The chip structure of the valves consists of three layers of PDMS and a glass slide. An extra PDMS 10:1 layer has been added to prevent delamination. The figure has been reproduced from Bossink et al. [40].

to other materials, such as Poly(methyl methacrylate) (PMMA), resulted in issues with trapped air bubbles. The details of these tests can be found in appendix B.

Due to the fabrication difficulties with Flexdym, it was decided to use PDMS, as this has already been proven to work for push-up Quake valves[34]. No experiments with hormones will be conducted in this work, so the permeability of PDMS is not an issue to demonstrate the proof-of-principle. In future experiments with hormones, a surface coating of the PDMS channel could help reduce the permeability of PDMS[39].

Since the flexible control layer will be made using PDMS, it was decided to use the same materials as used by Bossink et al.[34]. The valves will be made of PDMS and glass. All the chip layers can be seen in figure 4.1. An extra layer of PDMS is added between the control layer and the substrate. This layer improves the bond quality between the layers to prevent delamination [34].

4.1.2 Valve Dimensions

The valve dimensions should be chosen correctly, as the performance of the valves can vary greatly depending on the proportions of the dimensions[34]. The dimensions of the chip will affect the flow conditions and need to fulfil requirement 3a.

Figure 4.2 highlights five important valve dimensions. To determine what these dimensions should be, it should be known what other design aspects they affect. The first choice regarding the valve dimensions has been made with the sensors in mind. As discussed in section 3.1.3, two sensors will be placed next to each other, with a distance between them that is equal to $1\mu L$ in the channel dimensions. It was decided to take $1cm$ as the distance between the sensors, as this would leave space for the sensors without making the dimensions too small for fabrication. Based on this, the cross-sectional area of the flow channel should be $10^{-7}m^2$.

There are various combinations of flow channel height and width that will result in a cross-sectional area of $10^{-7}m^2$. A wider and lower channel results in a better functioning valve[34]; however, this also increases the footprint of the system. The width of the control channel was also found to affect the performance[34]. A valve test chip was designed to determine the ratio of flow channel width to flow channel height and the ratio of control

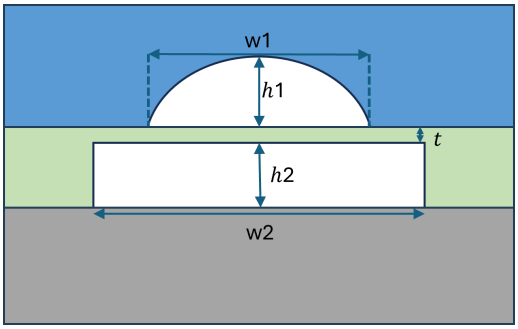

Figure 4.2: The push-up quake valve design with five dimensions highlighted. The height ($h1$) and width ($w1$) of the flow channel, the height ($h2$) and width ($w2$) of the control channel, and the thickness (t) of the membrane separating the two channels.

channel width to flow channel height. The aspect ratios can be seen in table 4.1. 25 different valves will be tested in total. All of these dimensions for the flow channel fulfil requirement 3a, as their Reynolds' numbers are in the order of magnitude of 10^{-2}. An overview of the exact dimensions can be found in appendix D.

Table 4.1: Overview of the channel dimensions in the valve test chip. The columns show the ratio between the control channel width $W2$ and the flow channel height H. The rows show the ratio between the flow channel width $W1$ and the flow channel height H. Note that the crossectional area of the flow channel is always equal to $10^{-7}m^2$.

$W2/H$ $W1/H$	2	2.5	3	3.5	4
2	Valve 1	Valve 2	Valve 3	Valve 4	Valve 5
2.5	Valve 6	Valve 7	Valve 8	Valve 9	Valve 10
3	Valve 11	Valve 12	Valve 13	Valve 14	Valve 15
3.5	Valve 16	Valve 17	Valve 18	Valve 19	Valve 20
4	Valve 21	Valve 22	Valve 23	Valve 24	Valve 25

The 25 valves in the valve test chip will be tested, and the valve design with the smallest footprint, which is consistently gas-tight, will be used for the droplet generator. The results of these tests will be discussed in chapter 5.

The final dimension that has not been discussed is the membrane thickness. In the work of Bossink et al. [40], a protocol to create $60\mu m$ thick membranes for the push-up quake valves was described. This same protocol was recreated. However, it resulted in thinner membranes. The membrane was measured to be only $10\mu m$ thick during testing. The valves could still be operated, so it was decided to continue with these thinner membranes. The measurements of the membrane thickness can be found in appendix C.3.

4.1.3 Valve Fabrication

The fabrication protocol of the push-up Quake valves is adapted from Bossink et al.[34]. During testing, some small changes were made to the original protocol. The full protocol can be found in appendix C.1. In section 4.1.1, a four-layer structure was discussed, which can be seen again in figure 4.3. The top two layers of PDMS will be created with their own moulds, and the bottom layer of PDMS will be spin-coated on top of the glass layer.

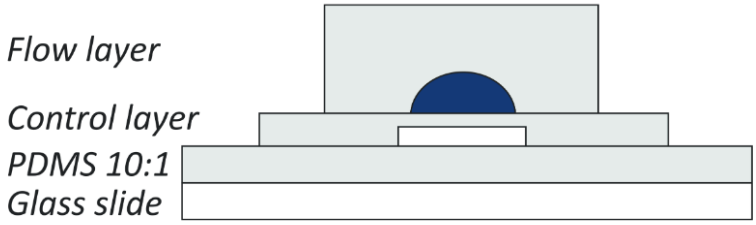

Figure 4.3: The chip structure of the valves consists of three layers of PDMS and a glass slide. An extra PDMS 10:1 layer has been added to prevent delamination. The figure has been reproduced from Bossink et al. [40].

The two moulds that will be needed to make the flow layer and the control layer will be created from PMMA using a micromill. The designs of these moulds have been made in Fusion 360 and can be found in appendix D.2. The tools used to create the moulds range from $8mm$ down to $1mm$ in diameter and are operated at a $20000RPM$ with a feed rate of $400mm/min$.

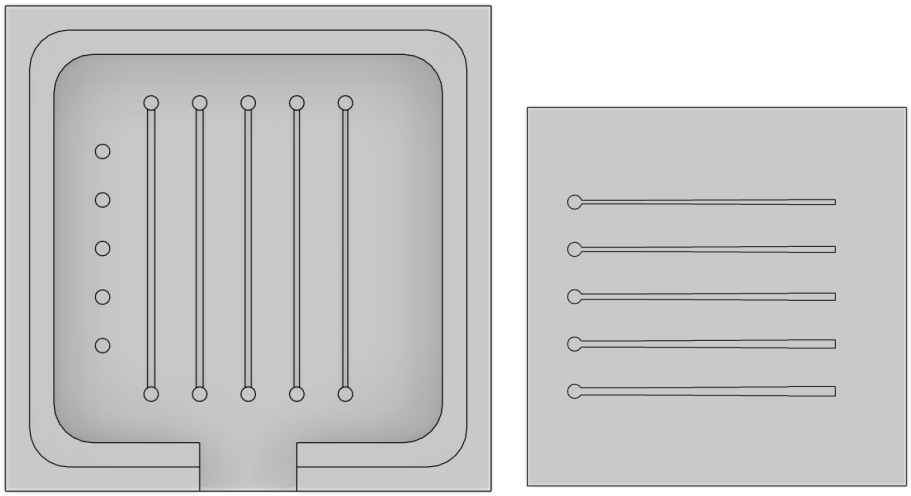

(a) (b)

Figure 4.4: Top view of the moulds used to create the valve test chip. A) the mould used to make the flow layer has a basin into which PDMS can be easily poured. B) the mould used to make the control layer is mostly flat, allowing for spin coating.

The moulds are shown in figure 4.4. The flow layer mould (Figure 4.4a) is made to allow for the easy pouring of PDMS. An opening at the side of the mould allows easy removal of the cured flow layer; during curing, it will be closed using scotch tape. The flow layer mould contains the five flow channels with an inlet and outlet for each channel. The inlets of the control layer are also there to help with the alignment during bonding. The control layer mould (Figure 4.4b) is made for spin coating. The flat surface will be coated by spinning an uncured PDMS at $750RPM$ for one minute.

The control layer will be the thinnest layer, and the membrane on top of the control channels will be the most fragile part of the device. As discussed in section 4.1.2, this layer

was measured to be $10\mu m$ thick. During testing with the control layer mould, a defect was found. The edges of the channels had upstanding edges, roughly $10\mu m$ in height. This resulted in leaks between the control channel and the flow channel. The defects were removed using an acetic acid treatment of the PMMA mould. The treatment is discussed in appendix C.2.

4.2 Sensor

The sensor will measure the difference in light intensity as light is refracted away from the sensor due to the difference in refractive index as discussed in section 3.2.2. The larger the difference, the more light is refracted away from the sensor; when air is in the channel, the measured light intensity should be lower than when there is water in the channel. To increase the sensitivity of the sensor, the only light reaching the sensor should have travelled through the channel. Any other light will not carry information regarding the medium in the channel and would only reduce the sensitivity of the sensor. As such, the sensor will be operated in a dark room, and the light source will be partially shielded to only illuminate a small part of the channel. In this section, the components needed to create the sensor will be chosen, and the circuit is designed to be used to amplify the signal before the microcontroller measures it.

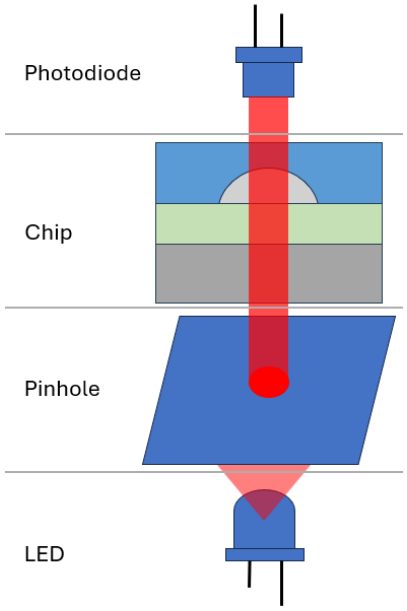

Figure 4.5: Schematic drawing of the sensor, on top, an LED shines light through a pinhole onto the channel; the light passes through either the plug of water or the plug of air and finally reaches the photodiode below.

4.2.1 Choice of Components

It was decided to use an LED for the light source and a photodiode for the sensor since they are small, cheap, efficient, and easy to use. LEDs emit light in a specific range of wavelengths, and photodiodes receive light in a specific range of wavelengths. As such, they should be chosen to be complementary to one another. As for the wavelengths, it was decided to use visible light as this is safer to use. Specifically, red-coloured LEDs and

complementary photodiodes were chosen. In the red part of the visible light spectrum, the difference in attenuation between water and air is the largest [41][42], although at the length scales of the device, this will most likely be negligible.

LED: WURTH ELEKTRONIK 151051RS11000[43]

Photodiode: AMS OSRAM GROUP SFH 203[44]

The sensor design is shown in figure 4.5. As can be seen in the figure, a pinhole is added to prevent the extra light from the LED from reaching the sensor, which could reduce the sensitivity. The diameter of the pinhole was chosen after some testing and is $750\mu m$.

4.2.2 Sensor holder

One more part is needed to use the sensor: a holder that aligns the LED, the pinhole, the photodiode, and the chip. For the first tests, a holder was made from PMMA for a single sensor using a scroll saw and a drill. The first version can be seen in figure 4.6a. Two support structures support the chip. The alignment structure aligns the LED, the photodiode and the pinhole. The chip is free to be moved and can be aligned manually.

A second, more stable sensor holder was made for the final system based on the first sensor holder. This second holder holds two sensors that are spaced $1cm$ apart. It was made using a micromill to create more precise shapes. It has an indentation into which the pinhole is placed. This makes it easier to align the pinhole and provides a more even base on which the chip can be placed. The structure is supported only on one side to create more space for the chip's inlets and outlets.

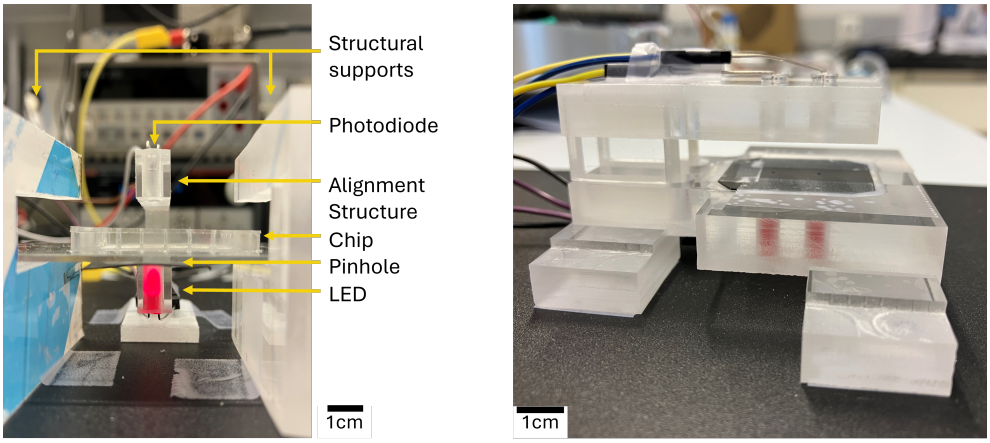

(a) (b)

Figure 4.6: A) The first sensor holder that will be used to test the sensor itself. The subcomponents of the sensor holder and the chip are pointed out. B) The second sensor holder that will be used with the final chip. It contains two sensors, and its structure is more stable than the first sensor holder.

4.2.3 Transimpedance Amplifier

The photodiode will create a current on the order of $1\mu A$. The data acquisition device measures voltages from $0V$ to $5V$. Thus, the current signal needs to be changed to a voltage signal and amplified. The exact amplification needed is unknown and will have to be tested. For this purpose, a transimpedance amplifier will be used. The circuit can be seen in figure 4.7a [45]. For this circuit, a LM358P amplifier will be used. This is a small dual-channel operational amplifier that will be able to amplify the signals of both photodiodes in the final system [46].

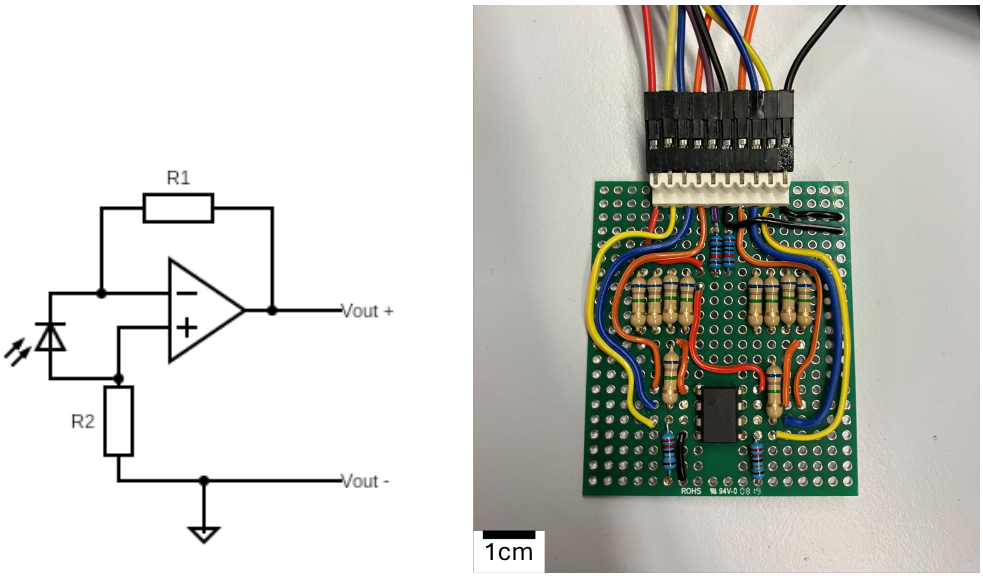

(a) (b)

Figure 4.7: A) The transimpedance amplifier circuit that is used to amplify the photodiode current. B) The soldered circuit contains two transimpedance amplifiers that will be used to amplify the signals of the two sensors.

The circuit's gain is equal to $R1$, and it should be chosen large enough to allow the data acquisition to measure the voltage swing consistently. The photodiode will need to be connected to the ground, and this is done with resistor $R2$. The value of this resistor will determine the offset of the voltage swing from the ground. Since the required gain is unknown, both resistor values will have to be chosen during testing. For these tests, the circuit will be built on a breadboard. Based on these tests that will be discussed in chapter 5, the final design of the circuit was found. This final design was soldered to create a more stable circuit. The soldered circuit is shown in figure 4.7b. Soldering the circuit also helped reduce the electromagnetic interference caused by the electricity grid, which will be further discussed in chapter 5.

4.3 setup

This section will discuss how the test setup for our system will be made. This setup will be used to test the valves, sensors and the droplet generator. As such, it will need to contain pumps for the fluid flows, a system to control the valves, and data acquisition to read out the sensors' measurements.

4.3.1 Equipment

In section 3.2.3, three pieces of equipment were mentioned. All the equipment will be connected to a computer, acting as the central controller of the setup.
The first piece of equipment is the pressure pump. A Bronkhorst IQ+Flow system[47] was used for this. This system measures and controls the pressure of the flow, resulting in a pump that produces a very stable pressure output. It was connected directly to the computer and controlled using Bronkhorst software. The system has two channels and can handle both the pressure pump for the air and the water input. The second piece of equipment is the solenoid valve system, which will pressurise the control channels to actuate the push-up quake valves. For this, Festo MH1 solenoid valves (Festo)[48] will be used. These valves can switch at a frequency of $20Hz$, which gives the system good control over the flow. Although fast for valves, these valves will be the slowest part of the system. The MH1 is connected to the computer through a WAGO 750 controller to control the valves. The communication with the valves is done through the MODBUS protocol[49] using the PyModbus[50] package in Python.
The third piece of equipment is the Analog Discovery 2 (AD2)[51]. This will be used to read out the voltage signals created by the sensors. With a sample rate of $100Msamples/s$ and a resolution of $0.32mV$, it will be more than capable of measuring these signals. It will be connected directly to the computer and controlled using Python. A block diagram of the setup is shown in figure 4.8.

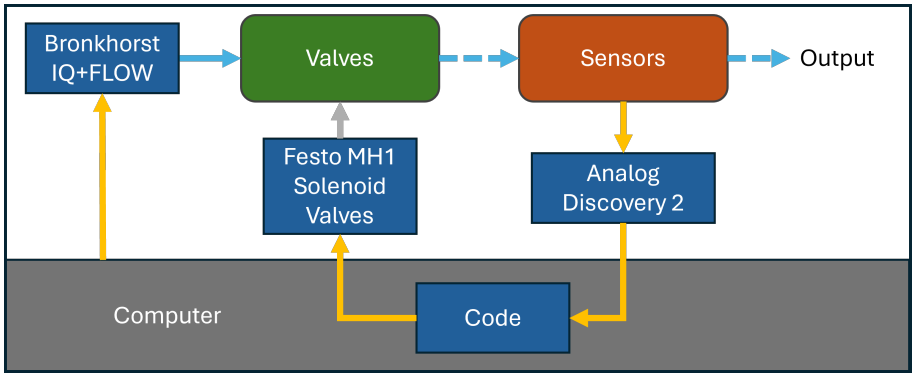

Figure 4.8: Block diagram showing how the various components of the system interact. The Bronkhorst IQ+Flow pressure pumps pump the fluid into the system. The valves are controlled using the Festo MH1 solenoid valves based on the measurements of the sensor read out by the Analog Discovery 2.

4.3.2 Code

The AD2 and the Festo will be controlled using Python. To control the AD2, a GitHub repository created by Digilent[52] will be used. A more complex method will be used to control the Festo. The Festo will be controlled directly through the Modbus protocol, which adds some complexity to the code. PyModbus[50] handles most of the work needed to communicate with Modbus. The remaining issue is that the Festo needs to be continuously updated. A small pause in these updates will cause the Festo to open all of its valves, which would disrupt our entire system. To allow for these updates, the code is multithreaded. One thread is asynchronous and updates the Festo whenever it can, and it does this based on the commands sent by the second thread. The second thread is responsible for the rest. It reads the sensors and sends commands to the first thread accordingly. It also ensures that the timing of the plug creation fits requirement 2a. The complete code can be seen in appendix E.

4.4 Sample Dispersion

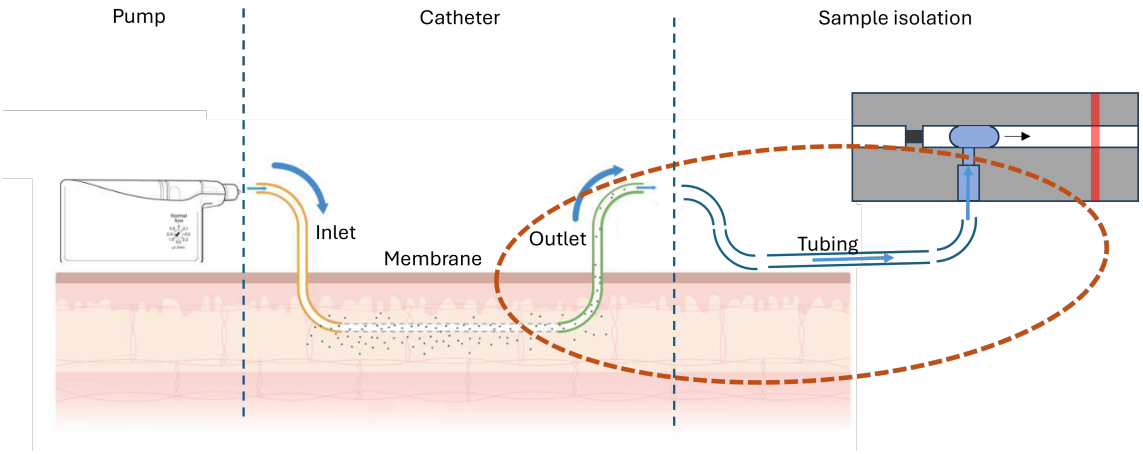

Figure 4.9: Diagram of how the sampling system is connected to the catheter and pump, the section that is modelled is circled in red. The figure is adapted from Upton et al. [12].

So far, the individual components, how they are connected, how their dimensions affect flow conditions and how material choice could help reduce crossover have been discussed. However, an important aspect of crossover still needs to be discussed. This system will create plugs by actively controlling the valves. As such, the user has complete control over the flow speeds and timing of the valves. Before the sample reaches the sample isolation stage, the flow speeds and how they are controlled greatly affect the sample dispersion. This stage is highlighted in figure 4.9. It includes the catheter output [22], the tubing between the catheter and the chip [8], and the channel in the chip before the sample isolation. The sections have the following dimensions:

- Catheter outlet:

  Length : 10 cm

  Diameter : 380 μm

  Volume : 11.3 μL

- Tubing:

  Length : 1 cm

  Diameter : 120 μm

  Volume : 0.11 μL

- Channel:

  Length : 5 mm

  Height : 189 μm

  Width : 756 μm

  Volume : 0.36 μL

It has been decided that the system will create one droplet every five minutes. During these five minutes, the system will create a plug of $1\mu L$ of sample, add $1\mu L$ of additives and push this plug into the sample store using gas. Depending on the flow rate of the sample stream, it might take 10 seconds to isolate and prepare a sample or nearly the full 5 minutes. When the sample stream is flowing, it is affected by Taylor dispersion, and when it is stationary, it is affected by diffusion. This section discusses a MATLAB model that uses the theory from section 2.2.3 to model the dispersion of a concentration pulse before it reaches the sample isolation.

4.4.1 The model

The derivation of the Taylor dispersion equation, is in essence based on the idea of a channel's chemical impulse response. It is the response or chemical profile that is leaving the channel outlet, starting with an impulse or Dirac Delta function at t=0 at the inlet. In this case the impulse consists of an (infinitely) small plug of high concentration at the channel inlet, while the remainder of the channel is filled with liquid at zero concentration. Figure 4.10 shows an example of impulse responses. It shows the effect of flow speed on the Taylor dispersion; all of the profiles represent the concentration profile after passing through the same channel length but at different flow speeds. For the channel dimensions, the diameter of the catheter outlet was used. This outlet has a diameter of 380 μm. For the channel length, 8.8mm was used, as this results in a total volume of $1\mu L$.

In figure 4.10, the concentration is spread over a larger length than the channel itself. This is because the formula used in the model returns the concentration profile over time as it passes by the end of the channel. Since the samples are stored in set volumes of $1\mu L$, the focus should be on having the original concentration peaks spread out over as small a volume as possible, which can be directly translated to having the concentration peaks spread out over as small a channel length as possible. To show how the flow speed affects the channel length over which the concentration peak is spread out, it was decided to use distance on the x-axis in figure 4.10. The figure shows that at higher flow rates, the concentration peak will be spread out further.

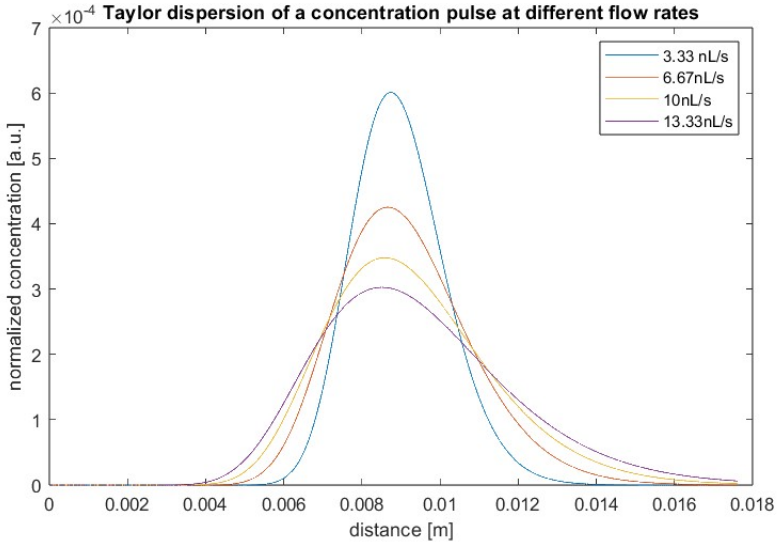

Figure 4.10: Impulse responses of the same channel at different flow speeds.

In linear systems theory, calculating an impulse response is the first step in calculating the response of the entire system to any input. Using the convolution of a chemical input profile and the chemical impulse response of a channel, the chemical output profile of that channel can be calculated. This reduces the channel's effect on the chemical profile to a single convolution. When the impulse response is used like this, it is referred to as the transfer function of the system. Using the output of one channel as the input for the next channel makes it possible to model the entire system. In that case, all the transfer functions of the entire system are combined into one large transfer function.

To model the effect of the system before the sample isolation, transfer functions of the highlighted channels as shown in figure 4.9 are needed. The sample stream in this part of the system can be paused, which is also taken into account when modelling the system's behaviour. When the flow in this part of the system is stopped, diffusion will occur, and when the flow moves, Taylor dispersion will occur. By combining all the transfer functions of the different channels and flow conditions, the effect of the system before the sample isolation can be calculated. Using these mathematics, a MATLAB model was made. The script can be found in appendix F.1.

4.4.2 Expected Sample Dispersion

With the model, the expected effect on the chemical profile between the porous part of the catheter until the sample isolation can be studied. For the input chemical profile, the system starts with the porous part of the catheter filled with a concentration of 1 and the rest of the system with a concentration of 0. The volume in the porous part of the catheter is $1.96\mu L$. For the flow rates, each fluid added during the sample isolation got the same amount of time. So the sample stream, the additive flow and the gas flow are all opened for $1/3$ of the five-minute sample period, which results in a flow rate of $10nL/s$.

The result is shown in figure 4.11. The figure shows the chemical profile over time as

it enters the sample isolation stage. The bars represent the individual samples in $1\mu L$ plugs. As mentioned before, the input chemical profile had all of the concentration in just under $2\mu L$, which could have been stored in two plugs. After traversing the channels up to the sample isolation, the concentration is spread out over 19 different plugs. This shows that the samples are already spread over many other samples before they are isolated, which is far from ideal. Improving upon this has been left outside the project's scope, but in appendix F, a closer look has been taken at the model's results, and some suggestions for improving the system are discussed.

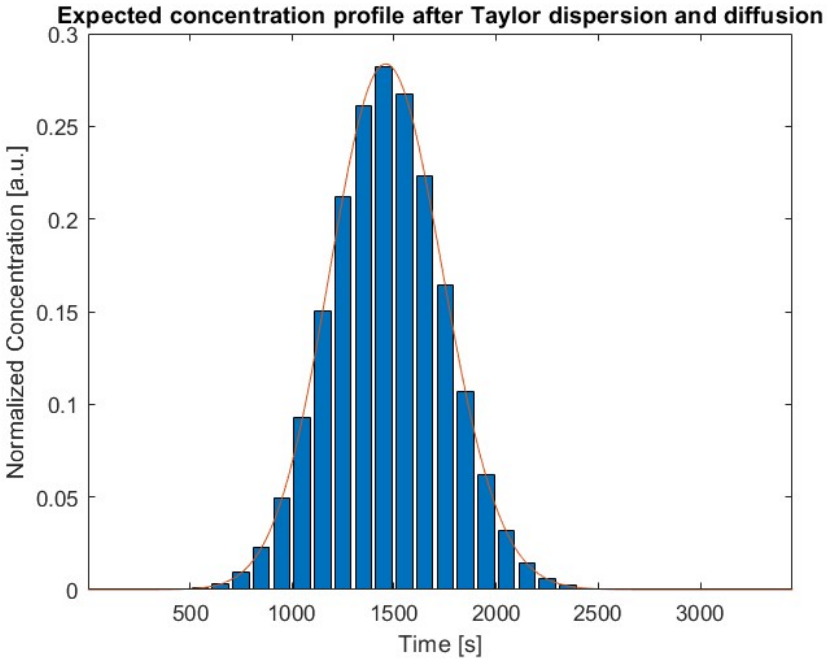

Figure 4.11: Expected sample dispersion at a flow rate $10nL/s$, the orange line shows the concentration profile over time, and the blue bars show how this profile would be distributed over plugs of $1\mu L$.

4.5 final chip design

Now that all components are done, the final chip containing the droplet generator and the injector can be designed. The results of the valve and sensor tests, which will be discussed in chapter 5, have also been incorporated into the final design. The chip contains the T-junctions and valves that comprise the droplet generator and injector. The sensors are not part of the chip, but there are alignment marks to align with the points where the volume reaches $1\mu L$ and $2\mu L$.

The design can be seen in figure 4.12. The figure overlaps the fusion designs of the flow layer with the control layer. The flow of fluids in the chip is shown using blue arrows. The flows start in the three inlets, I1, I2 and I3 and flow towards the outlet. Each flow is controlled by a valve, V1, V2a & V2b and V3, respectively. The second flow has a second valve as a backup since V2a is very close to V1, and there could be bonding issues. Each valve has its' own pressure inlet. Finally, there are the two alignment marks for the sensors S1 and S2. The locations where the sensors will be positioned have been marked by two

red circles.
The first sensor is positioned at $1cm$ and the second at $2cm$ from the first T-junction. The sensor holder will be positioned on the right side of the device. Because of this, the outlet channel needs to be curved towards the top side to be able to place the outlet.

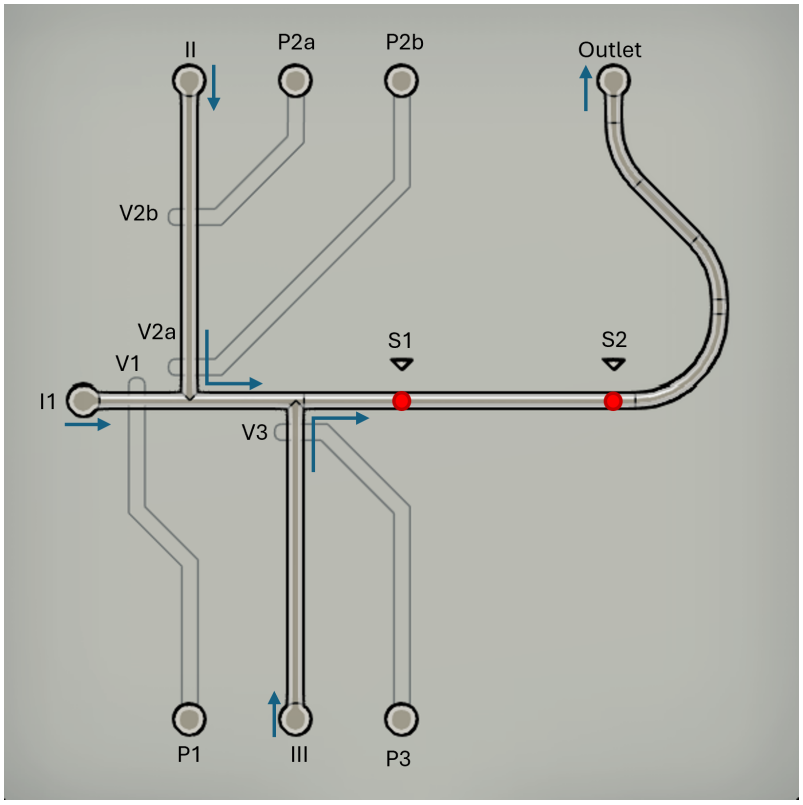

Figure 4.12: The final chip design, the image is an overlay of the control and flow layer designs in Fusion. The flow starts at the inlets I1, I2 and I3, and its direction is shown using blue arrows. The flow is controlled using valves V1, V2a, V2b and V3. The sensors are represented with red circles and aligned with the alignment structures S1 and S2.

Chapter 5

Results and Discussion

5.1 Valve

To determine the correct dimensions for the valves, a valve test chip was designed in section 4.1. The valves on the valve test chip were tested one at a time. The control channel was pressurised to pressures of 500, 750 and $1000mBar$. The flow channel was driven using a pressure pump set to $25mBar$. The channel before the valve was filled with air, followed by water. If, after one minute, no fluid had moved, it was deemed gas tight. If the air was escaping and the water reached the valve, another minute was waited; if no water passed through the valve, it was deemed water tight. Figure 5.1 shows an example of such a test.

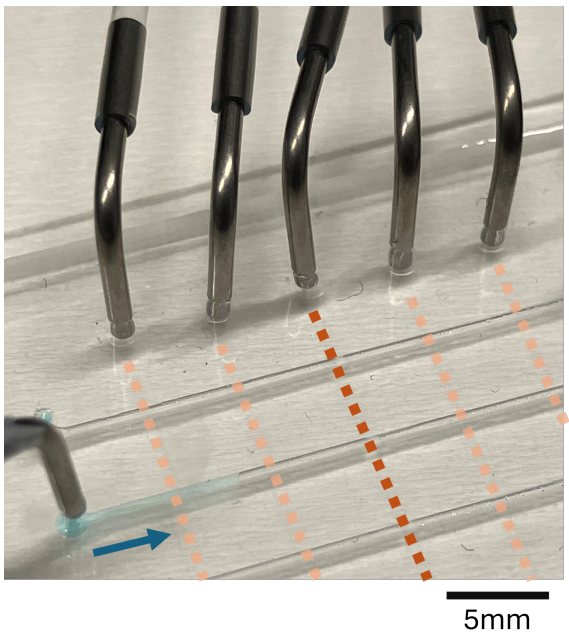

Figure 5.1: An example of the valve tests performed on the valve test chip. The dotted lines are placed over the control channels to visualise their locations better. The dark orange dotted line represents the pressurised middle control channel. The blue arrow indicates which flow channel is pressurised and in what direction the flow should flow. The water in the flow channel is dyed using blue food dye; air is stuck in the channel between the valve and the water, indicating that the valve is gas tight.

Table 5.1 shows the results from all 25 valve designs in the first chip tested at a pressure of 750$mBar$ on the control channels. The complete results of the valve tests of three chips can be found in appendix D.3.

Table 5.1: Table containing the results of the valve tests with valve test chip 1 with a control channel pressure of 750$mBar$.

750 mBar	Control channels:	1	2	3	4	5
Flow channels:	Aspect Ratio:	4	3.5	3	2.5	2
1	4	Gas Tight	Gas Tight	Gas Tight	Water Tight	Leaking
2	3.5	Gas Tight	Gas Tight	Gas Tight	Leaking	Leaking
3	3	Water Tight	Water Tight	Water Tight	Leaking	Leaking
4	2.5	Leaking	Leaking	Leaking	Leaking	Leaking
5	2	Leaking	Leaking	Leaking	Leaking	Leaking

The first chip's results show a clear trend: higher aspect ratios of the flow and control channels result in better-performing valves. By increasing the pressure in the control channel, more valves are able to stop the airflow. This trend was expected based on the findings of Bossink et al.[34]. Unlike the valves in their work, these valves have aspect ratios above two and also function with actuation pressures below 900$mBar$.

Table 5.2: Table containing the results of the valve tests with valve test chip 2 with a control channel pressure of 500$mBar$.

500 mBar	Control channels:	1	2	3	4	5
Flow channels:	Aspect Ratio:	4	3.5	3	2.5	2
1	4	Gas Tight	Water Tight	Water Tight	Water Tight	Water Tight
2	3.5	Gas Tight	Gas Tight	Gas Tight	Water Tight	Water Tight
3	3	Water Tight	Water Tight	Gas Tight	Water Tight	Water Tight
4	2.5	Water Tight	Water Tight	Gas Tight	Gas Tight	Leaking
5	2	Water Tight	Leaking	Gas Tight	Water Tight	Water Tight

The second and third chips were only tested at 500$mBar$ and were less predictable. Table 5.2 shows the results of the second chip. In general, the valves of this chip performed better, with fewer valves leaking. However, since there is no clear trend in what valve dimensions work best, there might be some inconsistencies in the fabrication of this chip. This variation between chips is non-ideal and shows that there is room for improvement in the robustness of the fabrication methods.

One valve design was gas tight in five of the six tests. In the remaining test, the valve could not be tested due to a leak in that flow channel, as nothing could be said about the performance of that valve. This most consistent valve has an aspect ratio of four for both the flow and the control channels. This valve will be used for the final chip design. The flow channel of this valve is 189 by 756 μm and the control channel of this valve is 100 by 756 μm.

5.2 Sensor

The sensor that will measure the size of the plugs must distinguish between water and air inside the channel. As discussed in section 4.2, a transimpedance amplifier is used to amplify the signal of the photodiode. The test setup discussed in section 4.2 was used to measure the transition from gas to water inside the flow channel. Based on these tests, the resistor values in the circuit were chosen, and the final circuit can be seen in figure 5.2a. Figure 5.2b shows the signal measured when water is pushed into a gas-filled channel. The signal shows a clear transition from one medium to the next.

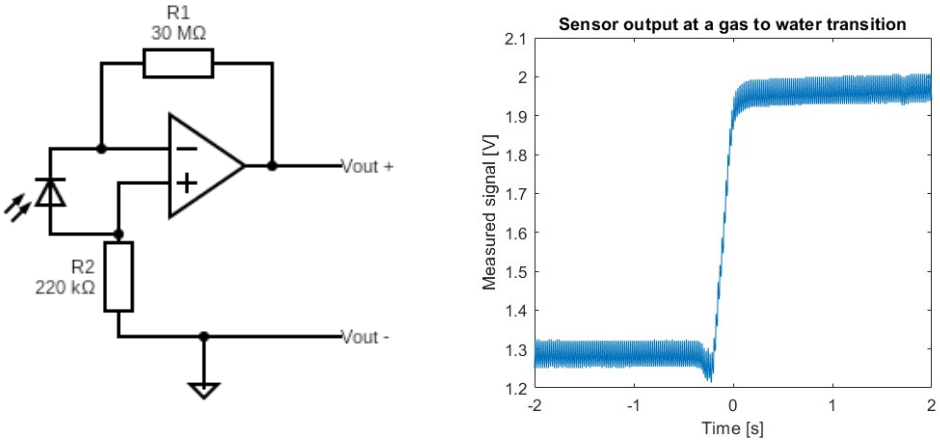

(a) (b)

Figure 5.2: A) The final circuit design of the transimpedance amplifier that is used to amplify the signal of the photodiode. B) The output of the complete sensor as the medium in the channel transitions from gas to water.

As discussed in section 4.2, the circuit for the final setup will be soldered and connected to a dual sensor setup that looks at two points in the same channel. Figure 5.3 shows the resulting outputs of this sensor setup. It shows how the sensors measure the change in channel medium from gas to water as water is pushed into a gas-filled channel.

One benefit of soldering the circuit can be seen by comparing figures 5.2 and 5.3. Figure 5.2 shows the signal output of an amplifier built on a breadboard. An unwanted signal at $50Hz$ can be seen, caused by ElectroMagnetic Interference (EMI) from the electricity grid. For the amplifier on the breadboard, this EMI is more significant; it has many long wires connecting the components, and each of these wires acts as an antenna which receives this EMI. The soldered circuit has only a handful of longer wires, and the difference in EMI can be clearly seen in figure 5.3. Because of this advantage, the circuit used for the final system was soldered.

In figure 5.3, it can also be seen that the two sensors do not produce the same output voltages. This difference is caused by an error during the soldering of the second amplifier. Some of the resistors that make up the feedback resistance have been short-circuited. This reduced the feedback resistance and, thus, the gain of the amplifier. Since the amplifier could still clearly distinguish between the two media, it was decided to continue with this amplifier.

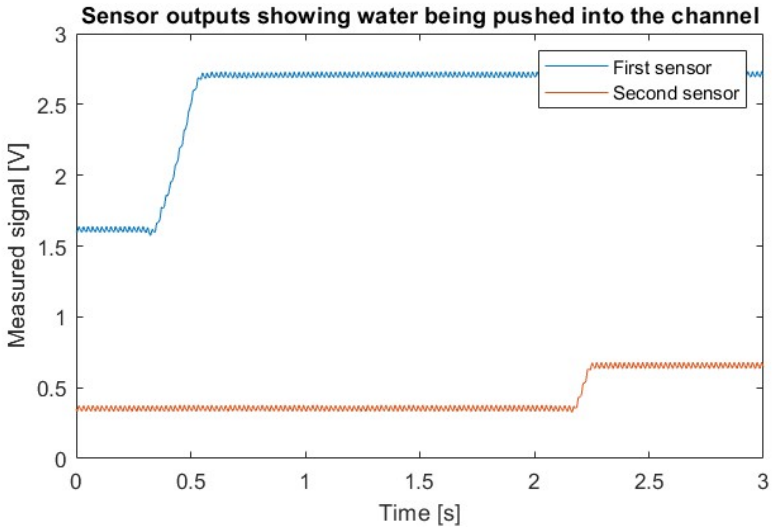

Figure 5.3: This figure shows the outputs of both sensors. They are looking at the same channel as water is slowly pushed into it. The sensors can measure this one at a time.

5.3 Final Chip

During the fabrication of the final chip, there were a few problems. The bonding of the PDMS layers was not as strong as it needed to be, and this caused leaking valves. Another issue that occurred was that during the punching of the inlets and outlets, the PDMS would tear, creating a leak.

The droplet generator could be tested despite the faulty valves by connecting two of the valve test chips to the final chip, as shown in figure 5.4b. The two valve test chips were used as external valves; the incoming flow was directed through the flow channels, and by controlling the pressure on the control channels, this flow could be turned on or off. Despite the broken valves on the final test chip, the T-junction and the alignment marks for the sensors could still be used, as shown in figure 5.4c. Together, the chips form a fully functioning droplet generator. The leaking inlets were glued closed at first using PDMS. This solution worked for a few minutes of testing before the inlets started leaking again. Then, they were glued closed using glue that hardens when exposed to ultraviolet light. This solution was good enough for a few more tests, but eventually, the inlets started leaking again. Because of this, the total number of plugs created was limited, and no clear quantitative statements about the performance could be made.

To test the performance of the active droplet generator with feedback, it was used to create plugs. The sample rate was set to one sample per 10 seconds. The created droplets were stored in $0.04in$ Tygon tubing $30cm$ long. The setup was as described in section 4.3 using the code from appendix E. The airflow and waterflow were pressurised with $125mBar$ and $75mBar$, respectively.

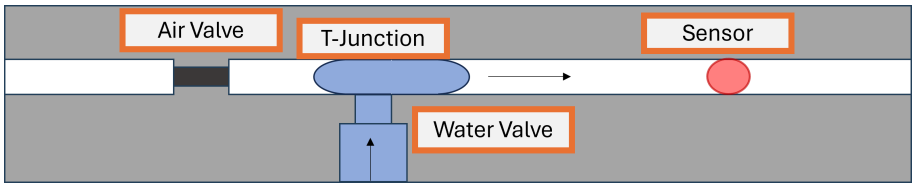

(a)

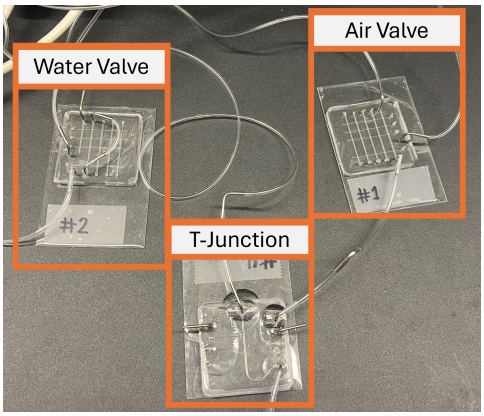

(b)

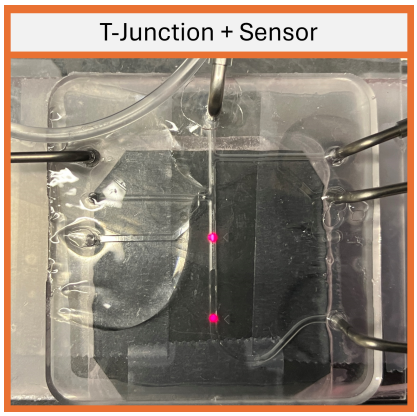

(c)

Figure 5.4: An overview of how the droplet generator was tested. A) A schematic drawing of the droplet generator and its components. B) The fluidics of the droplet generator, the two valves are used on separate valve test chips and the T-junction is on the final chip. C) The final chip that will be used as a T-junction on the sensor holder, the LEDs in the sensor are aligned with the flow channel and can be seen as red dots.

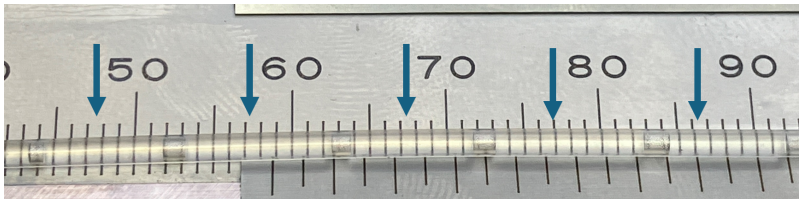

(a)

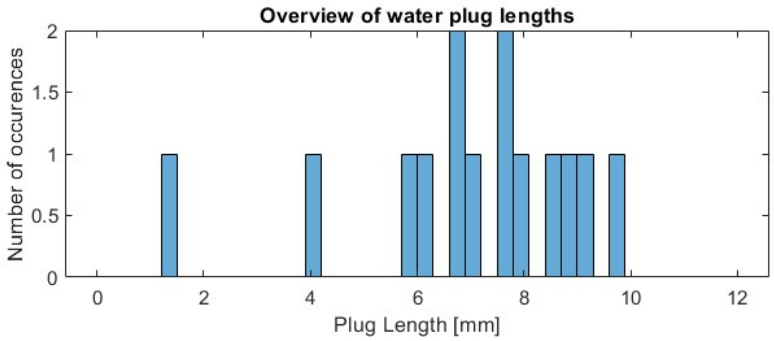

(b)

Figure 5.5: A) One of the photos used to determine the plug lengths. B) An overview of all measured water plug lengths

Figure 5.5a shows one example of the resulting plugs: the tubing is photographed on top of a calliper. The markings on the calliper, together with ImageJ, are used to measure the pixel lengths and lengths of the plugs. The complete length distribution of the plugs is shown in figure 5.5b. The plugs are divided into bins of $0.3mm$. Based on the tubing size, if the system were working as expected, it would have been filled with alternating plugs of air and water, each with a length of approximately $1.2mm$. However, this is not the case. The air plugs are almost the right size, but the water plugs are much longer. Taking a closer look at the length distribution, it seems like there is a periodicity to the plug lengths. It could be that the larger plugs are a combination of multiple smaller ones.

To understand what is happening, a closer look was taken at the droplet generator in operation. To study the behaviour of the droplet generator, it had to be taken out of the dark room. This meant that the sensor was no longer working and that the timings of the valves had to be controlled without feedback. A few things were changed in the system to get the droplet generator to create stable plug sizes. The output tube was shortened to a bit over $15cm$. This reduced the effect of the stored plugs and made stabilising the system significantly more manageable. The inlet tubes were also shortened. Originally, these were extra long to create a larger pressure drop, which would allow the flows to go slow enough to make full use of a sample rate of one sample per five minutes. However, extra tubing was no longer helpful since a much higher sample rate was used during these tests. The air and water flows were pressurised with a pressure of $2mBar$ and $10mBar$, respectively. The plugs were created by opening alternating which valve was open every second.

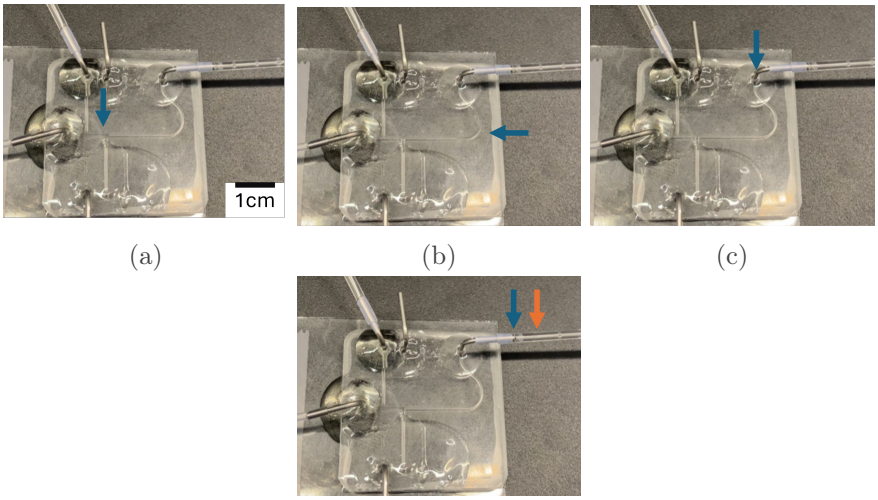

(a) (b) (c)

(d)

Figure 5.6: Frames from a video of the active droplet generator without feedback. The blue arrows indicate the location of the plug. The time between images is roughly $350ms$. In the image D) the plug is expected to be at the orange arrow. However, this is not the case; the plug seems stuck in the outlet.

During the tests without the sensor feedback, unexpected behaviour was seen. Figure 5.6 shows how, after a water plug is created, it moves down the channel and seems to get stuck in the outlet. In figure 5.6d, the plug finally enters the outlet. It appears that in the outlet, the air plug could pass by the water plug, and when the next water plug came along, they merged and entered the tubing.

During these tests without feedback, it was noticed that many small changes significantly affected the plug sizes. Pausing both flows before creating the next air and water plugs significantly increases the plugs' size, as can be seen in figure 5.7a. Allowing the air plugs to decompress seems to reduce the required pressure to push the next plug into the channel. Figure 5.7b shows the effect of slightly altering the height of the outlet tubing. The outlet tubing is moved up approximately $2cm$, this reduces the effect of gravity on the plugs and results in smaller plugs. Both of these effects show that minor variations in the system can greatly impact the output. Because of this, the system without feedback can be said to be unstable. The feedback might have been able to stabilise the system. However, this could not be tested, as the final chip also started leaking.

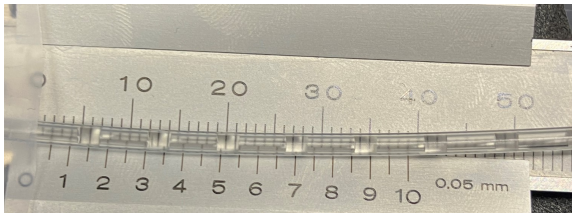

(a)

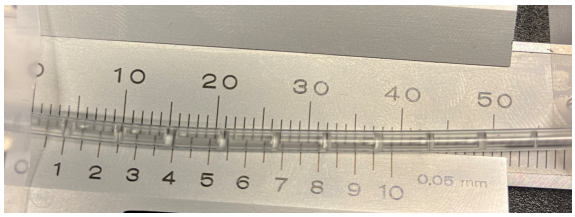

(b)

Figure 5.7: Variations in plug size created by the active droplet generator without feedback due to small changes in the system. A) When a pause was added to allow the compressed air plugs to decompress. B) When the output tube was pulled upwards by $2cm$.

Chapter 6

Conclusion

This work aimed to design, fabricate and test an on-demand integrated microfluidic microsample handling system for sample preparation and analysis that can operate at higher sample rates and with a smaller sample size than the current state-of-the-art. The system was to be designed to measure cortisol levels from the interstitial fluid. Due to the complexity of this aim, it was subdivided into four subgoals, which will be discussed individually in the coming sections.

6.1 The Requirements

Based on the aim of the system and the phenomena that affect it, eleven requirements were defined. They were split into three categories: The design context, the general technical specifications and the specifications of the temporal resolution. These requirements formed the basis on which all design choices were made.

6.2 The Conceptual Design

To fulfil the design requirements, two novel design concepts were introduced. (1) To create plugs of consistent volumes and with precise timing, an actively controlled droplet generator with feedback was designed. The droplet generator controls all incoming flows and uses feedback to determine when the plug has reached the correct size. This could allow the system to create consistent plugs from compressible and incompressible liquids in the chaotic environment of a portable device. (2) Using these same design principles, an actively controlled injector with feedback was designed to add consistent volumes of additives to each plug. These concepts will be made using a combination of push-up Quake valves and optical transmission sensors. To test the devices, a more extensive setup is needed, including pressure pumps, solenoid valves, and data acquisition.

6.3 The Physical Design

It was decided what materials and protocols would be used to fabricate the push-up quake valves. A valve test chip was designed to determine what dimensions would work well for the valves. It contained 25 different valves, and after tests, the best airtight valve design was chosen for the final design. The transmission sensor uses simple off-the-shelf components to realize a small and cheap design. The signals from the photodiodes are amplified using transimpedance amplifiers. The gain of the amplifiers was fine-tuned in

tests to fit well with the voltage range of the Analog Discovery 2 that would be used for data acquisition. The equipment for the setup was chosen and Python code was written to control the entire system. The code reads the sensor output and actuates the valves. A Matlab model was created that shows how the whole system is limited by spreading samples over the sample stream due to diffusion and Taylor dispersion before it reaches the sample isolation. The model showed that reducing the flow rate is the best way to minimise the crossover between samples before the sample isolation. With all subcomponents finished, the final PDMS chip, which includes both the droplet generator and the injector, was designed.

6.4 The Experimental Results

The tests done to determine the valve dimensions and to fine-tune the amplifier circuit were discussed. The results of these tests showed that both components worked. The valves were airtight, and the sensor could distinguish between water and gas. The fabrication of the final chip had a few issues which limited the total number of tests that could be performed. During these tests, the droplet generator was able to create droplets, but droplets seemed to recombine in the outlet. A second test showed this behaviour again when the system was operated without feedback. Since the final design was not validated, it has not been proven that the system fulfils the requirements, but the intermediate results are positive, and the design concept is a promising candidate for an on-demand microsample handling system.

Chapter 7

Outlook

The results thus far look promising, but there is still more research to be done before the on-demand microsample handling system can outperform the current state-of-the-art. This chapter will give an overview of what directions future research could take to improve upon the concept.

Experimental validation of the complete system

The first step for this system would be to validate that the concept works. So far, the sub-components all work, and the first tests with the system show promise. However, without full validation, the concept will remain only a concept. For this to work, the outlets should be redesigned to prevent any merging of plugs and the system should be tested and validated at a sample rate of one sample every 5 minutes.

Improving the PDMS fabrication protocols

During testing, it became clear that the current fabrication protocols were unreliable. For the final chip, only one out of four worked a bit, and even that one had multiple issues with the inlets and the valves. When these chips were produced, the lab where they were made was very busy, and multiple people had similar problems with their projects. One consistent issue was with bonding, which was thought to be caused by the plasma cleaner. It could be that the plasma cleaner could not create a good vacuum, leaving a significant amount of moisture in the chamber, which reduced the effectiveness of the treatment. Another aspect of the fabrication that should be improved is the very thin $10\mu m$ membrane, which was torn in multiple devices. Bossink et al. [40] described a protocol to create $60\mu m$ membranes, however we were unable to recreate this for this work. As mentioned before, redesigning the in- and outlets could also be beneficial, as these were also a cause of failure in the final chip.

Redesigning the amplifier for the sensor

The current amplifier circuit could amplify the photodiode signal enough that the AD2 could read it. However, the circuit was not perfect. The resistance of the feedback resistor was a higher order of magnitude than the internal resistance of the operational amplifier; although no problems with this were observed, this can cause unexpected behaviour of the circuit. The current circuit also used a resistor to ground, this created a small offset voltage, which served no purpose. If such an offset is needed a variable resistor might be a better choice, as this would provide more tunability. A redesign of the amplifier circuit,

using, for example, a multistage amplifier, could result in a more stable output and more energy-efficient sensor.

Creating a stable protocol to create Quake valves with Flexdym

In this work, the Quake valves were made using PDMS. PDMS has many disadvantageous properties, which could cause issues. In theory, Flexdym does not suffer from these issues; however, finding a stable fabrication protocol has proven difficult. If a stable protocol can be created, it would benefit this microsample handling system. It could reduce possible issues with the sorption of hormones and allow for the upscaling of production if the system becomes a product.

Investigate the sorption of hormones and the effect of surface coatings

An alternative to using Flexdym would be to coat the surface of the PDMS. To understand what properties such a surface coating should have, the sorption of hormones should be investigated.

Design a portable setup

For the on-demand microsample handling system to outperform the U-Rhythm, it should also be portable. The current setup uses a PC, pressure pumps, a solenoid valve system, and an AD2, which combined are not very portable. The system might use an on-chip peristaltic pump and pressure sensor to recreate the behaviour of a pressure pump, and the control could be done with a microcontroller. Miniaturising the entire setup and maximising its energy efficiency, would be an essential step for this system and similar devices.

Automate the sample introduction into analysis equipment

One crucial part of the system that has not been mentioned yet is the introduction of the samples into the analysis equipment. Once the sampler has done its work and gathered a full day's worth of samples, how are those samples extracted from the system and introduced into analysis equipment such as mass spectrometry systems? Using a combination of the valves and sensors described in this work a system could be made that could introduce the samples one at a time into capillary electrophoresis or liquid chromatography channels.

Acknowledgements

During this work, I was assisted by multiple people. I want to use this opportunity to thank them, as this thesis would not have been possible without them.

First and foremost, I want to thank **Mathieu** and **Jasper** for their supervision. Mathieu's insights and suggestions were invaluable in transforming a vague design concept into a fully worked-out final design. With the help of Jasper's knowledge of the labs at BIOS, I was able to turn this design into a (nearly) working prototype.

I want to thank **Gijs** and **Guinevere** for their feedback on my midterm and for being part of my graduation committee.

I want to thank **Loes** and **Josh** for the many discussions and critical questions, which helped focus my efforts and sharpen my rhetoric.

I want to thank **Dmytro** for helping me design my setup and the code that controlled it.

I want to thank **Amélie** and **Anke** for their introductions, suggestions and discussions regarding Flexdym, even though it did not make the final design.

And, finally, I want to thank all the other members of **BIOS** for the interesting and engaging time, not least because of the many slightly off-topic discussions during coffee breaks. I look forward to the coming years.

Disclaimer

During the preparation of this work, I used Chat GPT 3.5 for suggestions during coding, layout improvements of my final report and general searches for the proper terminology of fields of research with which I was not yet acquainted. I also made use of Grammarly Premium to help remove grammar, writing and style mistakes in my thesis. After using these tools, I thoroughly reviewed and edited the content as needed, taking full responsibility for the final outcome.

Bibliography

[1] F. S. Dhabhar, "The short-term stress response – Mother nature's mechanism for enhancing protection and performance under conditions of threat, challenge, and opportunity," en, *Frontiers in Neuroendocrinology*, vol. 49, pp. 175–192, Apr. 2018, ISSN: 00913022. DOI: 10.1016/j.yfrne.2018.03.004. [Online]. Available: https://linkinghub.elsevier.com/retrieve/pii/S0091302218300293 (visited on 06/15/2024).

[2] J. A. Sheng, N. J. Bales, S. A. Myers, *et al.*, "The Hypothalamic-Pituitary-Adrenal Axis: Development, Programming Actions of Hormones, and Maternal-Fetal Interactions," en, *Frontiers in Behavioral Neuroscience*, vol. 14, p. 601 939, Jan. 2021, ISSN: 1662-5153. DOI: 10.3389/fnbeh.2020.601939. [Online]. Available: https://www.frontiersin.org/articles/10.3389/fnbeh.2020.601939/full (visited on 05/16/2024).

[3] B. Taborsky, S. English, T. W. Fawcett, *et al.*, "Towards an Evolutionary Theory of Stress Responses," en, *Trends in Ecology & Evolution*, vol. 36, no. 1, pp. 39–48, Jan. 2021, ISSN: 01695347. DOI: 10.1016/j.tree.2020.09.003. [Online]. Available: https://linkinghub.elsevier.com/retrieve/pii/S0169534720302536 (visited on 05/16/2024).

[4] E. Young, J. Abelson, and S. Lightman, "Cortisol pulsatility and its role in stress regulation and health," en, *Frontiers in Neuroendocrinology*, vol. 25, no. 2, pp. 69–76, Jul. 2004, ISSN: 00913022. DOI: 10.1016/j.yfrne.2004.07.001. [Online]. Available: https://linkinghub.elsevier.com/retrieve/pii/S0091302204000184 (visited on 05/16/2024).

[5] S. L. Lightman and B. L. Conway-Campbell, "The crucial role of pulsatile activity of the HPA axis for continuous dynamic equilibration," en, *Nature Reviews Neuroscience*, vol. 11, no. 10, pp. 710–718, Oct. 2010, ISSN: 1471-003X, 1471-0048. DOI: 10.1038/nrn2914. [Online]. Available: https://www.nature.com/articles/nrn2914 (visited on 02/28/2024).

[6] D. E. Henley, J. A. Leendertz, G. M. Russell, *et al.*, "Development of an automated blood sampling system for use in humans," en, *Journal of Medical Engineering & Technology*, vol. 33, no. 3, pp. 199–208, Jan. 2009, ISSN: 0309-1902, 1464-522X. DOI: 10.1080/03091900802185970. [Online]. Available: http://www.tandfonline.com/doi/full/10.1080/03091900802185970 (visited on 01/11/2024).

[7] R. M. Torrente-Rodríguez, J. Tu, Y. Yang, *et al.*, "Investigation of Cortisol Dynamics in Human Sweat Using a Graphene-Based Wireless mHealth System," en, *Matter*, vol. 2, no. 4, pp. 921–937, Apr. 2020, ISSN: 25902385. DOI: 10.1016/j.matt.2020.01.021. [Online]. Available: https://linkinghub.elsevier.com/retrieve/pii/S2590238520300217 (visited on 01/12/2024).

[8] R. C. Bhake, J. A. Leendertz, A. C. E. Linthorst, and S. L. Lightman, "Automated 24-hours sampling of subcutaneous tissue free cortisol in humans," en, *Journal of Medical Engineering & Technology*, vol. 37, no. 3, pp. 180–184, Apr. 2013, ISSN: 0309-1902, 1464-522X. DOI: 10.3109/03091902.2013.773096. [Online]. Available: http://www.tandfonline.com/doi/full/10.3109/03091902.2013.773096 (visited on 12/14/2023).

[9] *Cortisol (Urine) - Health Encyclopedia - University of Rochester Medical Center*. [Online]. Available: https://www.urmc.rochester.edu/encyclopedia/content.aspx?contenttypeid=167&contentid=cortisol_urine (visited on 05/16/2024).

[10] J. L. Calvi, F. R. Chen, V. B. Benson, *et al.*, "Measurement of cortisol in saliva: A comparison of measurement error within and between international academic-research laboratories," en, *BMC Research Notes*, vol. 10, no. 1, p. 479, Dec. 2017, ISSN: 1756-0500. DOI: 10.1186/s13104-017-2805-4. [Online]. Available: http://bmcresnotes.biomedcentral.com/articles/10.1186/s13104-017-2805-4 (visited on 05/16/2024).

[11] *U-RHYTHM*, en-US. [Online]. Available: https://www.u-rhythm.co.uk (visited on 05/16/2024).

[12] T. J. Upton, E. Zavala, P. Methlie, *et al.*, "High-resolution daily profiles of tissue adrenal steroids by portable automated collection," en, *Science Translational Medicine*, vol. 15, no. 701, eadg8464, Jun. 2023, ISSN: 1946-6234, 1946-6242. DOI: 10.1126/scitranslmed.adg8464. [Online]. Available: https://www.science.org/doi/10.1126/scitranslmed.adg8464 (visited on 12/13/2023).

[13] R. C. Bhake, V. Kluckner, H. Stassen, *et al.*, "Continuous Free Cortisol Profiles—Circadian Rhythms in Healthy Men," en, *The Journal of Clinical Endocrinology & Metabolism*, vol. 104, no. 12, pp. 5935–5947, Dec. 2019, ISSN: 0021-972X, 1945-7197. DOI: 10.1210/jc.2019-00449. [Online]. Available: https://academic.oup.com/jcem/article/104/12/5935/5539981 (visited on 05/16/2024).

[14] R. Bhake, G. M. Russell, Y. Kershaw, *et al.*, "Continuous Free Cortisol Profiles in Healthy Men," en, *The Journal of Clinical Endocrinology & Metabolism*, vol. 105, no. 4, e1749–e1761, Apr. 2020, ISSN: 0021-972X, 1945-7197. DOI: 10.1210/clinem/dgz002. [Online]. Available: https://academic.oup.com/jcem/article/105/4/e1749/5570194 (visited on 05/16/2024).

[15] L. I. Stirrat, J. J. Walker, K. Stryjakowska, *et al.*, "Pulsatility of glucocorticoid hormones in pregnancy: Changes with gestation and obesity," en, *Clinical Endocrinology*, vol. 88, no. 4, pp. 592–600, Apr. 2018, ISSN: 0300-0664, 1365-2265. DOI: 10.1111/cen.13548. [Online]. Available: https://onlinelibrary.wiley.com/doi/10.1111/cen.13548 (visited on 05/16/2024).

[16] D. P. Fudulu, G. D. Angelini, F. F. Papadopoulou, *et al.*, "The Peacock study: Feasibility of the dynamic characterisation of the paediatric hypothalamic-pituitary-adrenal function during and after cardiac surgery," en, *BMC Cardiovascular Disorders*, vol. 20, no. 1, p. 245, Dec. 2020, ISSN: 1471-2261. DOI: 10.1186/s12872-020-01516-y. [Online]. Available: https://bmccardiovascdisord.biomedcentral.com/articles/10.1186/s12872-020-01516-y (visited on 05/16/2024).

[17] E. N. Behrend, R. J. Kemppainen, and D. W. Young, "Effect of storage conditions on cortisol, total thyroxine, and free thyroxine concentrations in serum and plasma of dogs," en, *Journal of the American Veterinary Medical Association*, vol. 212, no. 10, pp. 1564–1568, May 1998, ISSN: 0003-1488. DOI: 10.2460/javma.1998.212.10.1564. [Online]. Available: https://avmajournals.avma.org/view/journals/javma/212/10/javma.1998.212.10.1564.xml (visited on 06/10/2024).

[18] K. A. McGurk, B. Owen, W. D. Watson, *et al.*, "Heritability of haemodynamics in the ascending aorta," en, *Scientific Reports*, vol. 10, no. 1, p. 14 356, Sep. 2020, ISSN: 2045-2322. DOI: 10.1038/s41598-020-71354-7. [Online]. Available: https://www.nature.com/articles/s41598-020-71354-7 (visited on 06/11/2024).

[19] T. M. Squires and S. R. Quake, "Microfluidics: Fluid physics at the nanoliter scale," en, *Reviews of Modern Physics*, vol. 77, no. 3, pp. 977–1026, Oct. 2005, ISSN: 0034-6861, 1539-0756. DOI: 10.1103/RevModPhys.77.977. [Online]. Available: https://link.aps.org/doi/10.1103/RevModPhys.77.977 (visited on 06/11/2024).

[20] M. Gordic, "Theoretical Modeling of Cortisol Sensor," en, Oct. 2008.

[21] "Understanding Taylor Dispersion Analysis," Malver Instruments Limited, White Paper, 2015. [Online]. Available: https://www.atascientific.com.au/wp-content/uploads/2017/02/WP150609UnderstandingTDA.pdf.

[22] "66 Linear Microdialysis Catheter," M Dialysis AB, Datasheet, Apr. 2024. [Online]. Available: https://www.mdialysis.com/wp-content/uploads/2024/05/8010622J.pdf (visited on 06/12/2024).

[23] Department of Urology, Mersin City Research and Training Hospital, Mersin, Turkey, B. Saylam, S. Cayan, and Department of Urology, Mersin University Faculty of Medicine, Mersin, Turkey, "Do antioxidants improve serum sex hormones and total motile sperm count in idiopathic infertile men?" en, *Türk Üroloji Dergisi/Turkish Journal of Urology*, vol. 46, no. 6, pp. 442–448, Oct. 2020, ISSN: 21493235, 21493057. DOI: 10.5152/tud.2020.20296. [Online]. Available: https://www.urologyresearchandpractice.org/en/do-antioxidants-improve-serum-sex-hormones-and-total-motile-sperm-count-in-idiopathic-infertile-men-133656 (visited on 06/13/2024).

[24] "Droplet stability by using dSurf fluorsurfactant," Fluigent, Application Note. [Online]. Available: https://www.fluigent.com/wp-content/uploads/2022/01/droplet-stability-using-dsurf-fluorosurfactant_app-note.pdf (visited on 06/13/2024).

[25] J. Dolan, "When Should an Internal Standard be Used?" en, LCGC North America-06-01-2012, vol. 30, pp. 474–480, Jun. 2012, Publisher: MJH Life Sciences. [Online]. Available: https://www.chromatographyonline.com/view/when-should-internal-standard-be-used-0 (visited on 06/13/2024).

[26] P. Zhu and L. Wang, "Passive and active droplet generation with microfluidics: A review," en, *Lab on a Chip*, vol. 17, no. 1, pp. 34–75, 2017, ISSN: 1473-0197, 1473-0189. DOI: 10.1039/C6LC01018K. [Online]. Available: http://xlink.rsc.org/?DOI=C6LC01018K (visited on 01/16/2024).

[27] Z. Liu, J. Zhao, Y. Pang, and X. Wang, "Generation of droplets in the T-junction with a constriction microchannel," en, *Microfluidics and Nanofluidics*, vol. 22, no. 11, p. 124, Nov. 2018, ISSN: 1613-4982, 1613-4990. DOI: 10.1007/s10404-018-2144-3. [Online]. Available: http://link.springer.com/10.1007/s10404-018-2144-3 (visited on 06/18/2024).

[28] A. Etminan, Y. S. Muzychka, and K. Pope, "A Review on the Hydrodynamics of Taylor Flow in Microchannels: Experimental and Computational Studies," en, *Processes*, vol. 9, no. 5, p. 870, May 2021, ISSN: 2227-9717. DOI: 10.3390/pr9050870. [Online]. Available: https://www.mdpi.com/2227-9717/9/5/870 (visited on 06/07/2024).

[29] Sung Kwon Cho, Hyejin Moon, and Chang-Jin Kim, "Creating, transporting, cutting, and merging liquid droplets by electrowetting-based actuation for digital microfluidic circuits," en, *Journal of Microelectromechanical Systems*, vol. 12, no. 1, pp. 70–80, Feb. 2003, ISSN: 1057-7157. DOI: 10.1109/JMEMS.2002.807467. [Online]. Available: http://ieeexplore.ieee.org/document/1183744/ (visited on 06/18/2024).

[30] J. Cao, Q. An, Z. Liu, *et al.*, "Electrowetting on liquid-infused membrane for flexible and reliable digital droplet manipulation and application," en, *Sensors and Actuators B: Chemical*, vol. 291, pp. 470–477, Jul. 2019, ISSN: 09254005. DOI: 10.1016/j.snb.2019.04.102. [Online]. Available: https://linkinghub.elsevier.com/retrieve/pii/S0925400519306252 (visited on 06/18/2024).

[31] P. Thurgood, S. Baratchi, A. Arash, E. Pirogova, A. R. Jex, and K. Khoshmanesh, "Asynchronous generation of oil droplets using a microfluidic flow focusing system," en, *Scientific Reports*, vol. 9, no. 1, p. 10 600, Jul. 2019, ISSN: 2045-2322. DOI: 10.1038/s41598-019-47078-8. [Online]. Available: https://www.nature.com/articles/s41598-019-47078-8 (visited on 06/16/2024).

[32] S. Zeng, B. Li, X. Su, J. Qin, and B. Lin, "Microvalve-actuated precise control of individual droplets in microfluidic devices," en, 2009.

[33] A. R. Abate, T. Hung, P. Mary, J. J. Agresti, and D. A. Weitz, "High-throughput injection with microfluidics using picoinjectors," en, *Proceedings of the National Academy of Sciences*, vol. 107, no. 45, pp. 19 163–19 166, Nov. 2010, ISSN: 0027-8424, 1091-6490. DOI: 10.1073/pnas.1006888107. [Online]. Available: https://pnas.org/doi/full/10.1073/pnas.1006888107 (visited on 06/17/2024).

[34] E. G. B. M. Bossink, A. R. Vollertsen, J. T. Loessberg-Zahl, A. D. Van Der Meer, L. I. Segerink, and M. Odijk, "Systematic characterization of cleanroom-free fabricated macrovalves, demonstrating pumps and mixers for automated fluid handling tuned for organ-on-chip applications," en, *Microsystems & Nanoengineering*, vol. 8, no. 1, p. 54, May 2022, ISSN: 2055-7434. DOI: 10.1038/s41378-022-00378-y. [Online]. Available: https://www.nature.com/articles/s41378-022-00378-y (visited on 06/17/2024).

[35] S. De Winter, "deWinter_ma_tnw.pdf," English, M.S. thesis, University of Twente, Enschede, The Netherlands, Jul. 2022.

[36] M. N. Polyanskiy, "Refractiveindex.info database of optical constants," en, *Scientific Data*, vol. 11, no. 1, p. 94, Jan. 2024, ISSN: 2052-4463. DOI: 10.1038/s41597-023-02898-2. [Online]. Available: https://www.nature.com/articles/s41597-023-02898-2 (visited on 06/17/2024).

[37] M. W. Toepke and D. J. Beebe, "PDMS absorption of small molecules and consequences in microfluidic applications," en, *Lab on a Chip*, vol. 6, no. 12, p. 1484, 2006, ISSN: 1473-0197, 1473-0189. DOI: 10.1039/b612140c. [Online]. Available: https://xlink.rsc.org/?DOI=b612140c (visited on 06/07/2024).

[38] *Flexdym 2022 upgrade*, en-US. [Online]. Available: https://eden-microfluidics.com/flexdym/ (visited on 03/25/2024).

[39] A. T. Martier, Y. V. Maurice, K. M. Conrad, F. Mauvais-Jarvis, and M. J. Mondrinos, *Sex-specific actions of estradiol and testosterone on human fibroblast and endothelial cell proliferation, bioenergetics, and vasculogenesis*, en, Jul. 2023. DOI: 10.1101/2023.07.23.550236. [Online]. Available: http://biorxiv.org/lookup/doi/10.1101/2023.07.23.550236 (visited on 06/07/2024).

[40] E. Bossink, "Recreating the gut on-chip : Sensors and fabrication technologies for aerobic intestinal host - anaerobic microbiota research," en, ISBN: 9789036553995, PhD, University of Twente, Enschede, The Netherlands, Jul. 2022. DOI: 10.3990/1.9789036553995. [Online]. Available: http://purl.org/utwente/doi/10.3990/1.9789036553995 (visited on 11/14/2023).

[41] R. M. Pope and E. S. Fry, "Absorption spectrum (380–700 nm) of pure water II Integrating cavity measurements," en, *Applied Optics*, vol. 36, no. 33, p. 8710, Nov. 1997, ISSN: 0003-6935, 1539-4522. DOI: 10.1364/AO.36.008710. [Online]. Available: https://opg.optica.org/abstract.cfm?URI=ao-36-33-8710 (visited on 06/17/2024).

[42] E. O. Hulburt, "Attenuation of Light in the Lower Atmosphere*," en, *Journal of the Optical Society of America*, vol. 25, no. 5, p. 125, May 1935, ISSN: 0030-3941. DOI: 10.1364/JOSA.25.000125. [Online]. Available: https://opg.optica.org/abstract.cfm?URI=josa-25-5-125 (visited on 06/17/2024).

[43] "151051RS11000 Datasheet WL-TMRC THT Mono-color Round Color," Würth Elektronik, Datasheet. [Online]. Available: https://www.we-online.com/components/products/datasheet/151051RS11000.pdf (visited on 06/19/2024).

[44] "Radial T1 3/4 SFH 203," ams-OSRAM AG, Datasheet. [Online]. Available: https://look.ams-osram.com/m/67e1a90044b03ee9/original/SFH-203.pdf (visited on 06/19/2024).

[45] *How to Design Stable Transimpedance Amplifiers for Automotive and Medical Systems*, nl-nl. [Online]. Available: https://www.digikey.nl/nl/articles/how-to-design-stable-transimpedance-amplifiers-automotive-medical-systems (visited on 06/19/2024).

[46] "Industry-Standard Dual Operational Amplifiers," Texas Instruments, Datasheet. [Online]. Available: https://www.ti.com/lit/ds/symlink/lm2904ba.pdf?ts=1719990419976&ref_url=https%253A%252F%252Fwww.mouser.fr%252F (visited on 07/03/2024).

[47] "IQ+FLOW," BRONKHORST HIGH-TECH B.V., Brochure. [Online]. Available: https://www.bronkhorst.com/getmedia/3a590b01-5ef3-4972-a423-7bb43bc797f8/iqflow.pdf (visited on 06/19/2024).

[48] "Solenoid valves MH1, miniature," Festo BV., Datasheet. [Online]. Available: https://www.festo.com/media/pim/632/D15000100122632.PDF (visited on 06/19/2024).

[49] "MODBUS APPLICATION PROTOCOL SPECIFICATION V1.1b3," Modbus, Aplication protocol. [Online]. Available: https://modbus.org/docs/Modbus_Application_Protocol_V1_1b3.pdf (visited on 06/19/2024).

[50] *Welcome to PyModbus's documentation! — PyModbus 3.7.0dev2 documentation*. [Online]. Available: https://pymodbus.readthedocs.io/en/latest/ (visited on 06/19/2024).

[51] *Analog Discovery 2 Specifications - Digilent Reference*. [Online]. Available: https://digilent.com/reference/test-and-measurement/analog-discovery-2/specifications (visited on 06/19/2024).

[52] *Digilent/WaveForms-SDK-Getting-Started-PY*, original-date: 2021-12-07T10:05:14Z, Jun. 2024. [Online]. Available: https://github.com/Digilent/WaveForms-SDK-Getting-Started-PY (visited on 06/19/2024).

[53] "Application Note : Flexdym Chip Bonding," Eden Tech, Application Note. [Online]. Available: https://eden-microfluidics.com/wp-content/uploads/2021/03/Application-Notes-Flexdym-Bonding.pdf (visited on 06/20/2024).

Appendices

A Push-down Quake valve COMSOL

The push-down quake valve was modelled in COMSOL to understand how the stress is distributed over the valve. The valve was modelled using the Solid Mechanics physics domain and the PDMS material. The author can provide the simulation files upon request. The result can be seen in figure 1. The symmetry of the valve is used to reduce the complexity of the model, as only 1/4 of the valve has to be modelled to understand its behaviour. The top channel is pressurised with $5kPa$, and the thinnest part of the membrane is $50\mu m$ thick.

The stress in the membrane peaks near its centre; here, the membrane is deflected the most and needs to deform the most. The lower edges of the top channel have been rounded, helping reduce the stress near those edges. Without those rounded corners, the stresses were similar to those in the centre of the membrane. Depending on the fabrication method, these stresses could cause delamination of the valve layers. It is likely that the failures observed by Winter et al. [35] occurred in these parts of the valve. Since these stresses are inherent to the design, it was decided to use the more classical and robust push-up Quake valve.

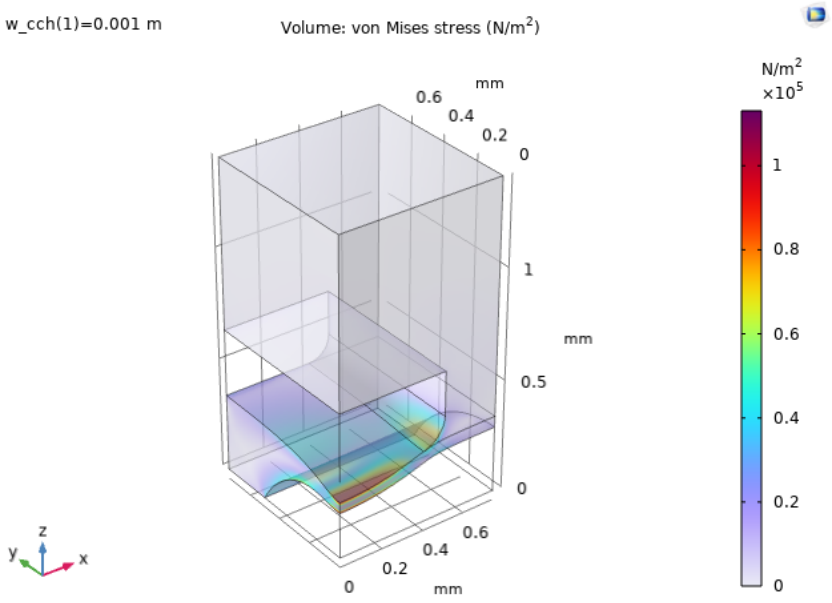

Figure 1: Stress distribution throughout a push-down Quake valve modelled in COMSOL. The top channel applies a pressure of $5kPa$ onto the membrane. This deforms the membrane, and with enough applied pressure, the channel closes.

B Flexdym

This appendix describes the tests on fabricating a control layer out of Flexdym. First, the protocol used to shape the Flexdym is described. The measured deformation and issues regarding the bonding of Flexdym will be shown.

B.1 Flexdym Fabrication

To form the Flexdym to the required shape, the Sublym machine was used as recommended by Eden Tech, the creators of Flexdym[38]. The Flexdym came in sheets of $250\mu m$ and sheets of $2mm$ thick. To form the Flexdym, the following steps should be taken:

1. Place the spacers that are needed inside of the machine (spacer size = Final thickness of the Flexdym + the Mould thickness + 4mm).
2. Preheat the machine.
3. Once the machine is heated, place the following stack of materials inside: One thin layer of non-stick material that can handle the heat (aluminium foil), the sheet of Flexdym precut to a similar size as the mould and the mould itself. Use heat-resistant gloves for this step.
4. Start the process (5-10 minutes at 165 degrees)
5. After the process is done, let the chip cool down before removing it from the mould.

Depending on the thickness of the Flexdym, the process might need to be hotter or longer in order to shape the material.

B.2 Flexdym Deformation

Flexdym expands when it is heated, so the material that forms to fit the mould will later contract and deform. The mould must be designed to take this into account. During testing, the deformation of the material was measured, and differences were found for the two types of Flexdym sheets. The measurements can be seen in figures 2 and 3. For the $250um$ sheet the deformation was 13.2% of the total thickness. For the $2mm$ sheet the deformation was 7.5% of the total thickness.

B.3 Flexdym Bonding

Flexdym needs to be bonded to PMMA to create valves. According to Eden Tech the company behind Flexdym, it should be able to bond to materials at room temperature [53], and some plasma treatment might be necessary to bond to glass. This never worked at all. The two materials were bonded by introducing a plasma treatment and following it up with a curing step; however, a lot of air was trapped between the layers. Multiple settings and cure times were tested, but none resulted in a good and clean bond between Flexdym and PMMA. In figure 4, an example of the resulting can be seen.

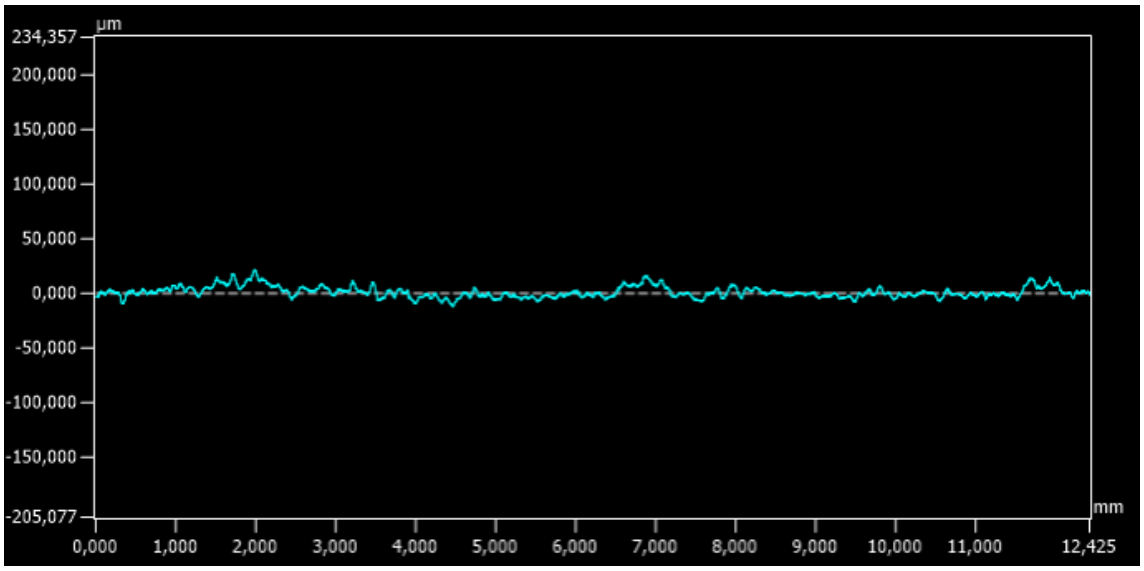

Figure 2: Deformation of 250um thick Flexdym sheet measured using a Keyence VK-X3000 3D LASER scan microscope, the surface should have been flat but has deformed.

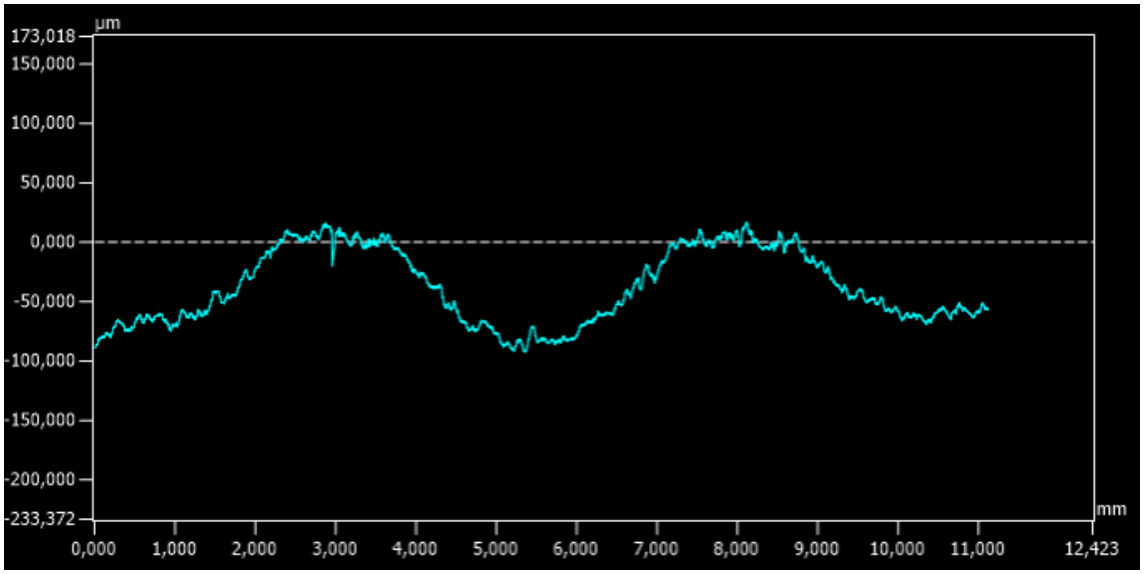

Figure 3: Deformation of 2mm thick Flexdym sheet measured using a Keyence VK-X3000 3D LASER scan microscope, the surface should have been flat, but has deformed significantly.

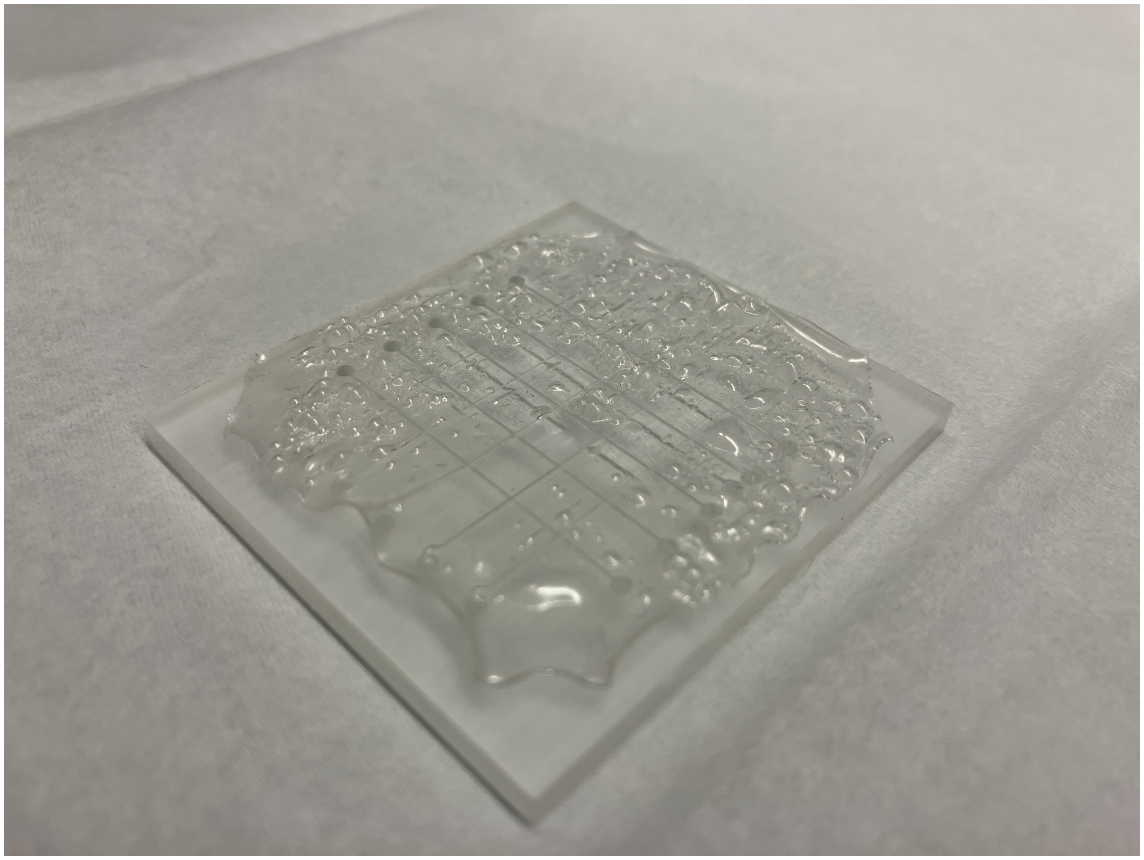

Figure 4: A piece of shaped $250\mu m$ Flexdym bonded onto a micromilled piece of PMMA, as can be seen, the result is not good, and there is a lot of air trapped between the layers.

C PDMS

In this appendix, the various aspects of making PDMS are discussed. The protocols used to make the final PDMS chip are described as mixing the PDMS and bonding the layers. The acetic acid treatment used to smoothen the control layer, the deformation of the final PDMS layers compared to the moulds and the membrane thickness is discussed.

C.1 PDMS Chip Fabrication Protocol

The PDMS chip fabrication protocol is adapted from Bossink et al. [40]. In their protocol, they bond the PDMS layers by only partially curing the layers before bonding. However, this was found to be unreliable, so it was decided to fully cure the layers and use plasma cleaning instead.

1. Prepare three mixtures of PDMS:
   (a) 7:1 (PDMS to curing agent) (mix and degas).
   (b) 10:1 (PDMS to curing agent) (mix and degas).
   (c) 20:1 (PDMS to curing agent) (mix and degas).
2. Prepare the flow layer mould by closing the sides with scotch tape.
3. Pour the 7:1 mixture into the flow layer mould.
4. Degas the mould until all air bubbles are gone (cycling the vacuum can help remove bubbles that have floated to the surface).
5. Cure the flow layer with mould for 2 hours.
6. Spin coat the 20:1 mixture onto the control layer mould (750 rpm for 60 seconds).
7. Cure the control layer with mould for 2 hours at 60 degrees.
8. Remove the flow layer from its mould.
9. Plasma clean the flow layer.
10. Plasma clean the control layer (still on the mould).
11. Bond the two layers, the flat side of the control layer onto the structured side of the flow layer, align using the inlets.
12. Cure the bonded layers for 2 hours at 60 degrees.
13. Spin coat the 10:1 mixture onto a glass slide (size of the glass slide should be at least 4cm x 4cm) (600 rpm for 60 seconds).
14. Cure the coated glass slide for 2 hours at 60 degrees.
15. Plasma clean the PDMS-coated glass slide.
16. Remove the control layer and flow layer from the control layer mould, and plasma clean the exposed structured side of the control layer.
17. Bond the two together and cure overnight at 60 degrees.
18. Punch the inlets and outlets into the PDMS (1mm hole puncher).

C.2 Mould Acetic Acid Treatment

During testing, it became clear that the control layer mould needed more processing before a reliable PDMS membrane could be made for the Quake valves. The height profile of the control layer mould was measured using a Keyence VK-X3000 3D LASER scan microscope. The original mould height profile can be seen in figure 5a. The first treatment that was tried was done by coating the surface of the mould with ethanol and placing the mould into a UV-oven. This was tried with curing periods of 30 seconds, 1 minute, 2 minutes, 4 minutes, 6 minutes and 10 minutes. However, as can be seen in figure 5b, which shows the mould after all of these treatments, this had no significant effect.

Next, a more aggressive treatment was used to smooth out the edges of the mould. The mould was covered in acetic acid and placed in a microwave for 3 minutes. Figure 5c shows the mould after one such treatment. Figure 5d shows the mould after two of these treatments. This last result was accepted, as the spikes no longer extended into the membrane when PDMS is spin-coated onto the mould.

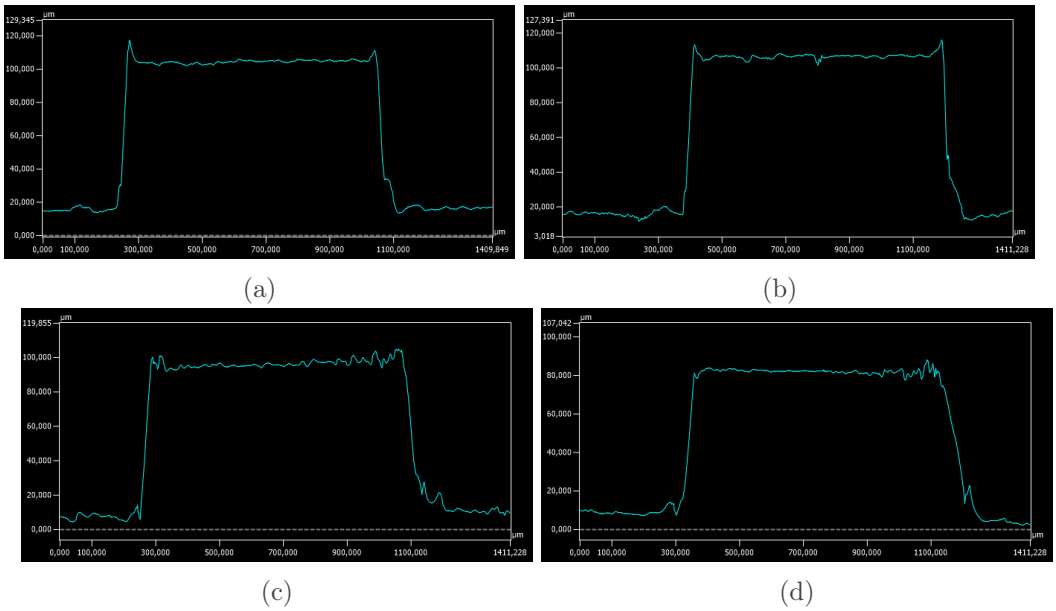

Figure 5: The changes in height profile of the PMMA control layer mould due to two types of treatment. The height profiles have been measured using a Keyence VK-X3000 3D LASER scan microscope A) The original mould. B) The mould after Ethanol UV-treatments. C) The mould after one acetic acid treatment. D) The mould after two acetic acid treatments.

C.3 Membrane Thickness

The membrane thickness was measured by taking a slice of the PDMS flow layer and control layer bonded together and measuring it with a Keyence VK-X3000 3D LASER scan microscope. The resulting image is shown in figure 6. The membrane is just over $10\mu m$ thick.

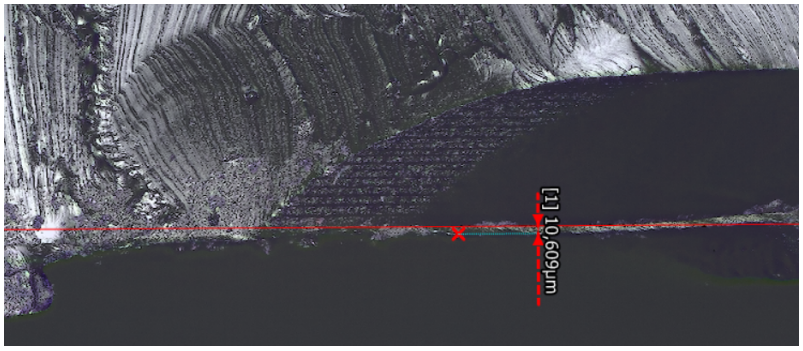

Figure 6: Image of a crosssection of the flow and control layer taken with a Keyence VK-X3000 3D LASER scan microscope. The thickness of the membrane is marked.

D Valve Test Chip

In this appendix, the details of the valve test chip are shown. This includes the exact dimensions of the channels, the Fusion files used for micromilling and an overview of all valve test results.

D.1 Channel Dimensions

Table 1: Table containing the dimensions of the valves. The aspect ratios refer to the ratio of the width of the flow or control channel to the height of the flow channel. The numbering of the valves is identical to that used in table 4.1 in section 4.1.

	Flow Channel			Control Channel		
Valve #	Aspect ratio	Height [um]	Width [um]	Aspect ratio	Height [um]	Width [um]
1	2	252	505	2	100	505
2	2	252	505	2.5	100	631
3	2	252	505	3	100	757
4	2	252	505	3.5	100	883
5	2	252	505	4	100	1009
6	2.5	232	579	2	100	463
7	2.5	232	579	2.5	100	579
8	2.5	232	579	3	100	695
9	2.5	232	579	3.5	100	811
10	2.5	232	579	4	100	927
11	3	215	644	2	100	430
12	3	215	644	2.5	100	537
13	3	215	644	3	100	644
14	3	215	644	3.5	100	752
15	3	215	644	4	100	859
16	3.5	201	703	2	100	402
17	3.5	201	703	2.5	100	502
18	3.5	201	703	3	100	603
19	3.5	201	703	3.5	100	703
20	3.5	201	703	4	100	803
21	4	189	757	2	100	378
22	4	189	757	2.5	100	473
23	4	189	757	3	100	567
24	4	189	757	3.5	100	662
25	4	189	757	4	100	757

D.2 Fusion Files

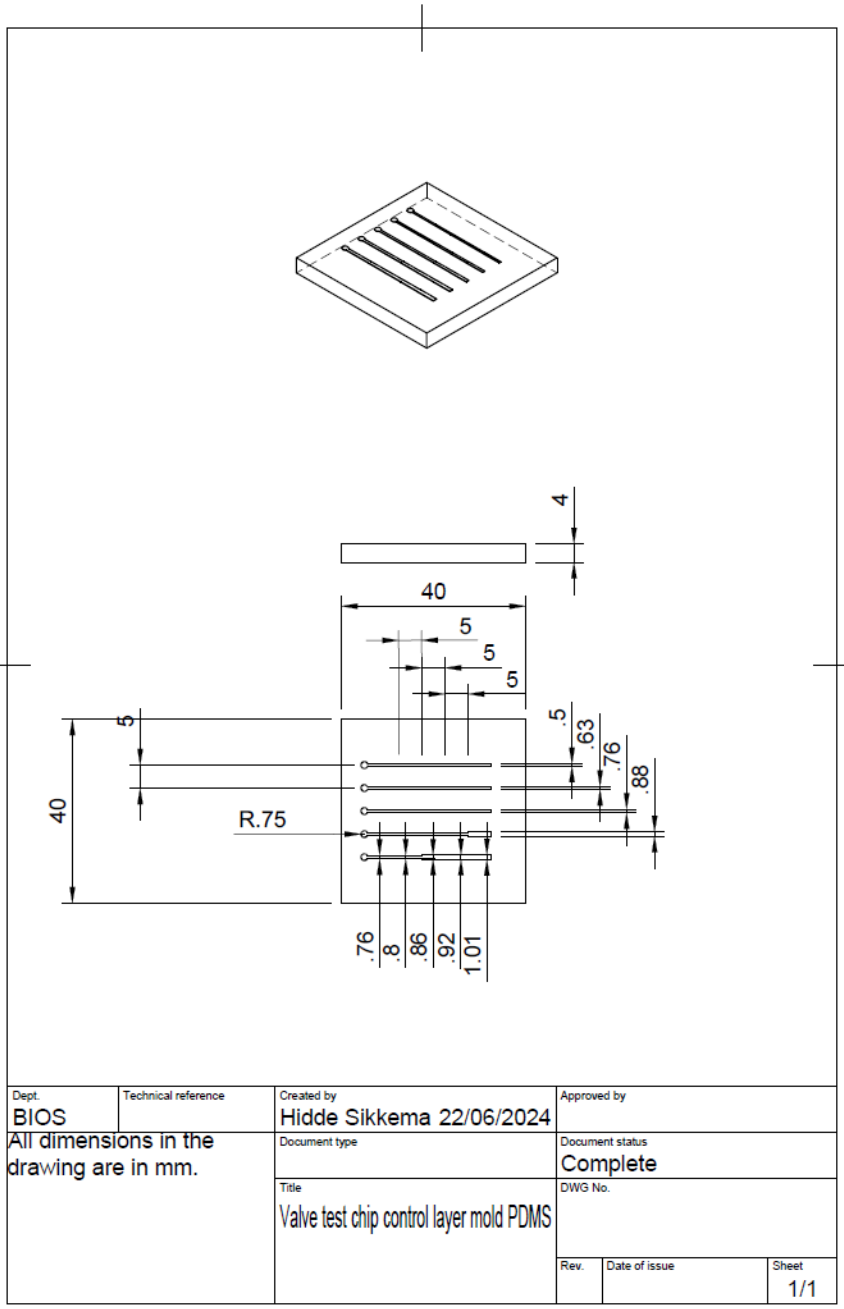

Dept.	Technical reference	Created by	Approved by
BIOS		Hidde Sikkema 22/06/2024	
All dimensions in the drawing are in mm.		Document type	Document status: Complete
		Title: Valve test chip control layer mold PDMS	DWG No.
			Rev. / Date of issue / Sheet: 1/1

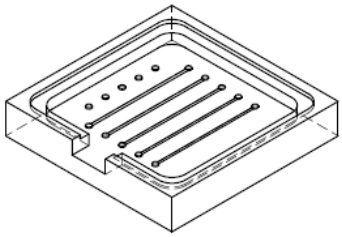

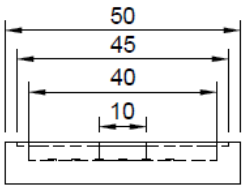

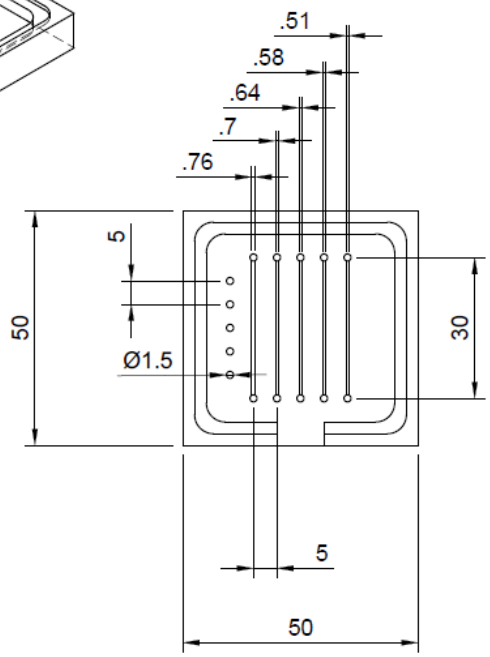

Dept.	Technical reference	Created by	Approved by
BIOS		Hidde Sikkema 22/06/2024	
All dimensions in the drawing are in mm.		Document type	Document status: Complete
		Title: valve test chip flow layer mold	DWG No.
			Rev. / Date of issue / Sheet: 1/1

D.3 Measurement results

Table 2: Table containing the results of the valve tests with valve test chip 1 with a control channel pressure of $500mBar$.

500 mBar	Control channels:	1	2	3	4	5
Flow channels:	Aspect Ratio:	4	3.5	3	2.5	2
1	4	Gas Tight	Water Tight	Leaking	Leaking	Leaking
2	3.5	Water Tight	Water Tight	Leaking	Leaking	Leaking
3	3	Water Tight	Water Tight	Leaking	Leaking	Leaking
4	2.5	Leaking	Leaking	Leaking	Leaking	Leaking
5	2	Leaking	Leaking	Leaking	Leaking	Leaking

Table 3: Table containing the results of the valve tests with valve test chip 1 with a control channel pressure of $750mBar$.

750 mBar	Control channels:	1	2	3	4	5
Flow channels:	Aspect Ratio:	4	3.5	3	2.5	2
1	4	Gas Tight	Gas Tight	Gas Tight	Water Tight	Leaking
2	3.5	Gas Tight	Gas Tight	Gas Tight	Leaking	Leaking
3	3	Water Tight	Water Tight	Water Tight	Leaking	Leaking
4	2.5	Leaking	Leaking	Leaking	Leaking	Leaking
5	2	Leaking	Leaking	Leaking	Leaking	Leaking

Table 4: Table containing the results of the valve tests with valve test chip 1 with a control channel pressure of $1000mBar$.

1000 mBar	Control channels:	1	2	3	4	5
Flow channels:	Aspect Ratio:	4	3.5	3	2.5	2
1	4	Gas Tight	Gas Tight	Gas Tight	Gas Tight	Leaking
2	3.5	Gas Tight	Gas Tight	Gas Tight	Gas Tight	Leaking
3	3	Gas Tight	Gas Tight	Gas Tight	Gas Tight	Leaking
4	2.5	Gas Tight	Gas Tight	Water Tight	Leaking	Leaking
5	2	Leaking	Leaking	Leaking	Leaking	Leaking

Table 5: Table containing the results of the second set of valve tests with valve test chip 1 with a control channel pressure of $750mBar$. Valves marked with an x have a leak in one of the channels and are no longer working.

750 mBar	Control channels:	1	2	3	4	5
Flow channels:	Aspect Ratio:	4	3.5	3	2.5	2
1	4	Gas Tight	Gas Tight	Gas Tight	Water Tight	x
2	3.5	Gas Tight	Water Tight	Gas Tight	Water Tight	x
3	3	Water Tight	Water Tight	Water Tight	Leaking	x
4	2.5	Water Tight	Water Tight	Leaking	Water Tight	x
5	2	Water Tight	Water Tight	Leaking	Water Tight	x

Table 6: Table containing the results of the valve tests with valve test chip 2 with a control channel pressure of $500mBar$.

500 mBar	Control channels:	1	2	3	4	5
Flow channels:	Aspect Ratio:	4	3.5	3	2.5	2
1	4	Gas Tight	Water Tight	Water Tight	Water Tight	Water Tight
2	3.5	Gas Tight	Gas Tight	Gas Tight	Water Tight	Water Tight
3	3	Water Tight	Water Tight	Gas Tight	Water Tight	Water Tight
4	2.5	Water Tight	Water Tight	Gas Tight	Gas Tight	Leaking
5	2	Water Tight	Leaking	Gas Tight	Water Tight	Water Tight

Table 7: Table containing the results of the valve tests with valve test chip 3 with a control channel pressure of $500mBar$.Valves marked with an x have a leak in one of the channels and are no longer working.

500 mBar	Control channels:	1	2	3	4	5
Flow channels:	Aspect Ratio:	4	3.5	3	2.5	2
1	4	x	x	x	x	x
2	3.5	Gas Tight	Gas Tight	Gas Tight	x	Gas Tight
3	3	Water Tight	Gas Tight	Gas Tight	x	Gas Tight
4	2.5	Water Tight	Water Tight	Water Tight	x	Gas Tight
5	2	Water Tight	Gas Tight	Gas Tight	x	Gas Tight

E Setup Control Code

```
import threading
import time
import asyncio
import tracemalloc
import pymodbus.client as ModbusClient
from ctypes import *
import numpy
import math
from pymodbus import (
    ExceptionResponse,
    ModbusException,
    pymodbus_apply_logging_config,
)

##############################################
""" Define global variables """

running = False
paused = True
festo_ready = False
additive = False
update_festo_active = False

# Define bytes for the Festo for opening and closing specific valves
byte0 = [
    False,
    False,
    False,
    True,
    True,
    True,
    True,
    True
]
byte1 = [
    True,
    False,
    False,
    True,
    True,
    True,
    True,
    True
]
byte2 = [
    False,
    True,
    True,
    True,
    True,
    True,
    True,
    True
]
byte3 = [
    True,
    True,
    False,
```

```
    True,
    True,
    True,
    True,
    True
]
byte = byte0
td = 0.05

########################################
""" Define Festo Functions"""


async def run_async_simple_client():
    """" Function to start the Festo client """
    global running, festo_ready, byte
    """ Run async client. """
    # activate debugging
    # pymodbus_apply_logging_config("DEBUG")
    print("get client")
    client = ModbusClient.AsyncModbusTcpClient('172.16.17.1')

    print("connect to server")
    await client.connect()
    # test client is connected
    assert client.connected

    # loop writing correct state to the Festo valves
    print("Start controlling valves")
    await festo_write(client)
    print("Stop controlling valves")

    print("close connection")
    client.close()


async def festo_write(client):
    """ Function that keeps the festo valves actuated """
    global running, festo_ready
    festo_ready = True
    while running:
        await client.write_coils(0, byte)


########################################
""" Define AD2 Functions"""


def ad2_setup():
    """ Function to set up the analog discovery 2"""
    dwf = cdll.dwf

    hdwf = c_int()
    secLog = 0.00001  # logging rate in seconds
    nSamples = 2000

    version = create_string_buffer(16)
    dwf.FDwfGetVersion(version)
    # print("DWF Version: " + str(version.value))

    # print("Opening first device")
```

```
    dwf.FDwfDeviceOpen(c_int(-1), byref(hdwf))

    if hdwf.value == 0:
        szerr = create_string_buffer(512)
        dwf.FDwfGetLastErrorMsg(szerr)
        print(str(szerr.value))
        print("failed to open device")
        return False, False, False

    dwf.FDwfDeviceAutoConfigureSet(hdwf,
                                   c_int(0))
    # 0 = the device will only be configured when FDwf###Configure is called

    # set up acquisition
    dwf.FDwfAnalogInChannelEnableSet(hdwf, c_int(0), c_int(1))
    dwf.FDwfAnalogInChannelRangeSet(hdwf, c_int(0), c_double(5))
    dwf.FDwfAnalogInAcquisitionModeSet(hdwf, c_int(1))  # acqmodeScanShift
    dwf.FDwfAnalogInFrequencySet(hdwf, c_double(nSamples / secLog))
    dwf.FDwfAnalogInBufferSizeSet(hdwf, c_int(nSamples))
    dwf.FDwfAnalogInConfigure(hdwf, c_int(1), c_int(0))

    # wait at least 2 seconds for the offset to stabilize
    time.sleep(2)

    # begin acquisition
    dwf.FDwfAnalogInConfigure(hdwf, c_int(0), c_int(1))

    return True, dwf, hdwf,


def ad2_read(dwf, hdwf, old_s1, old_s2):
    """ Function to read out the measurements of the sensors using the AD2 """
    nSamples = 2000
    sts = c_byte()
    rgdSamples1 = (c_double * nSamples)()
    rgdSamples2 = (c_double * nSamples)()
    cValid = c_int(0)

    dwf.FDwfAnalogInStatus(hdwf, c_int(1), byref(sts))
    dwf.FDwfAnalogInStatusSamplesValid(hdwf, byref(cValid))

    dwf.FDwfAnalogInStatusData(hdwf, c_int(0), byref(rgdSamples1), cValid)
    dwf.FDwfAnalogInStatusData(hdwf, c_int(1), byref(rgdSamples2), cValid)

    av1 = numpy.average(rgdSamples1)
    av2 = numpy.average(rgdSamples2)
    # print(av1)

    if time.time() % 5 < 0.002:
        sensor1_water = not old_s1

    if old_s1 == 2:
        sensor1_water = (av1 > 1.5)
    elif old_s1:
        sensor1_water = (av1 > 1.4)
    else:
        sensor1_water = (av1 > 1.6)

    if old_s2 == 2:
        sensor2_water = (av2 > 0.5)
    if old_s2:
```

```
        sensor2_water = (av2 > 0.45)
    else:
        sensor2_water = (av2 > 0.55)

    return sensor1_water, sensor2_water, av1, av2


def ad2_close(dwf, hdwf):
    """ Function to close the AD2 """
    dwf.FDwfAnalogOutConfigure(hdwf, c_int(0), c_int(0))
    dwf.FDwfDeviceCloseAll()


########################################
""" Define clock"""


def clock(t0, period):
    """ Function to check if the system should create a new plug """
    t1 = time.time()
    if t0 == 0:
        # start up
        return 1, t1
    elif t1 - t0 < period:
        # too early
        return 0, t0
    elif t1 - t0 >= 2 * period:
        # too late
        return 2, t1
    else:
        # ready for next plug
        return 1, t1


########################################
""" Define parallel threads """


def festo_thread():
    """Thread containing asynchronous code to control Festo MH1 miniature valve system."""
    asyncio.run(
        run_async_simple_client()
    )


def main_thread():
    """ Thread that controls the setup """
    global running, paused, byte

    # Notify other threads that the system has started
    running = True

    # Start the AD2
    ad2_ready, dwf, hdwf = ad2_setup()

    # Define starting values of variables
    state = 1
    t0 = 0
    t1 = 0
    period = 10
    sensor1 = 2
```

```
sensor2 = 2

# Create loop that can be stopped by user input
while running:
    # Create loop that can be paused by user input and errors
    if not paused:
        # Read out sensor data
        sensor1, sensor2, av1, av2 = ad2_read(dwf, hdwf, sensor1, sensor2)

        # Check current state of the system and act accordingly
        if state == 1:
            # Water plug formation state
            byte = byte1
            # Check if the water plug has reached the first sensor
            if sensor1:
                byte = byte0
                # Check if the injector should be used
                if additive:
                    state = 2
                else:
                    state = 3

        elif state == 2:
            # Additive injection stage
            byte = byte2
            # Check if the combination of the water plug and additives has reached
            # the second sensor
            if sensor2:
                byte = byte0
                state = 3

        elif state == 3:
            # Air plug formation stage
            byte = byte3
            # Check if the air plug has pushed the water plug away from
            # the first T-junction
            if not sensor1:
                byte = byte0
                state = 0

        # Check if the system is ready to create a next water plug
        next_plug, t0 = clock(t0, period)
        if next_plug == 1:
            # System is ready to create the next plug
            if state == 0:
                t1 = time.time()
                state = 1
                print("State 1")
        elif next_plug == 2:
            # System is too slow, send an error message and pause the system
            paused = True
            print(f"The program has been paused since the system pressure "
                  f"is too low to keep the flow speed high "
                  f"enough to make plugs within {period} seconds")
    else:
        # System is paused, close all valves and wait on user input
        byte = byte0
# System has been stopped, close the AD2
ad2_close(dwf, hdwf)
```

```
def user_thread():
    """ Thread that waits for user input and uses it to interrupt the other threads"""
    global additive, running, paused

    # Ask the user if the injector stage should be used
    txt = input("Do you want to create plugs with additives? (y/n):")
    if txt == 'y':
        additive = True
    else:
        additive = False

    # Create loop that can be stopped by user input
    while running:
        if not paused:
            # Ask the user if they want to pause the program, this can be done at any time
            txt = input("To pause the program enter 'p':")
            if txt == 'p':
                paused = True
        else:
            # Ask the user to unpause or stop the program
            txt = input("To unpause the program enter 'p', to stop the program enter 's':")
            if txt == 'p':
                paused = False
            elif txt == 's':
                running = False


##########################################
""" Create the separate threads and await their completion"""

tracemalloc.start()
print("start parallel thread")
t1 = threading.Thread(target=festo_thread)
t1.start()
t2 = threading.Thread(target=main_thread)
t2.start()
t3 = threading.Thread(target=user_thread)
t3.start()
t1.join()
t2.join()
t3.join()
```

F Sample Dispersion Model

As discussed in chapter 4, section 4.4, a MATLAB model has been created to model the dispersion of the chemical profile before it reaches the sample isolation. The input chemical profile that starts at the porous part of the membrane is spread out significantly and crosses over into many other samples. This dilutes the original chemical profile and reduces its temporal resolution. To reduce this effect, here are a few suggestions.

Suggestion 1: As was discussed in section 4.4, the dispersion of the profile increases with increasing flow rate. The flow rate of the sample stream could be minimised, by taking more of the five-minute sample period to create the sample plug. This does mean the sample would be flowing most of the time, which could reduce the recovery rate of hormones from the interstitial fluid into the catheter.

Suggestion 2: The system is modelled using a transfer function. These transfer functions also have an inverse, which can be used to determine the system's input from its output. With this, the diluted and spread-out chemical profile could be used to determine what the original chemical profile looked like. However, it would require that all influences of the physical system be known. Loss of hormones due to sorption and the limit of detection of the analysis equipment would reduce the effectiveness of this method.

Suggestion 3: The final and most practical method would be to alter the system between the porous part of the membrane and the sample isolation. Figure 7 shows the contributions to the sample dispersion of the subsections of that system. It is clear that the catheter outlet is by far the biggest issue. It has a total volume of $11.3\mu L$, this is a large dead volume that is clearly a problem.

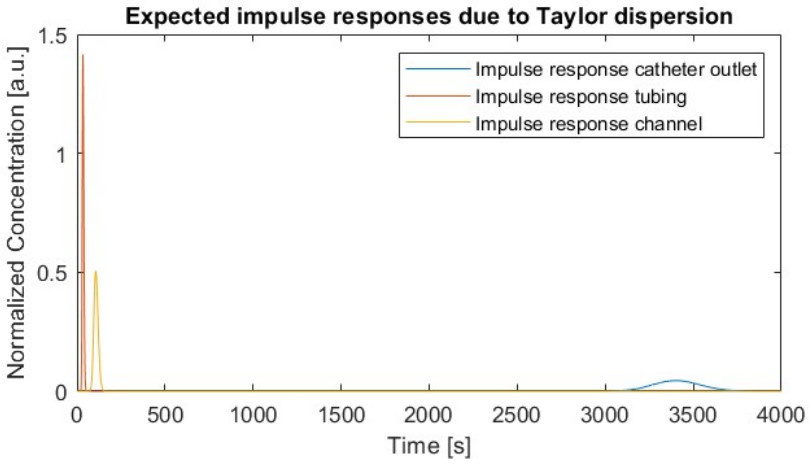

Figure 7: The impulse responses of the subsections of the system.

This could be solved by using a different catheter or altering the current one. By glueing a fused silica capillary into the outlet of the catheter, the dead volume would be significantly reduced. Take, for example, a capillary with an inner diameter of $100\mu m$, the volume of the catheter outlet would be reduced to only $0.79\mu L$, and the resulting chemical profile can be seen in figure 8. It is clearly a very effective method of reducing the spread and dilution. One big drawback of this approach is that the new or altered catheter must be approved for medical use before it can be used.

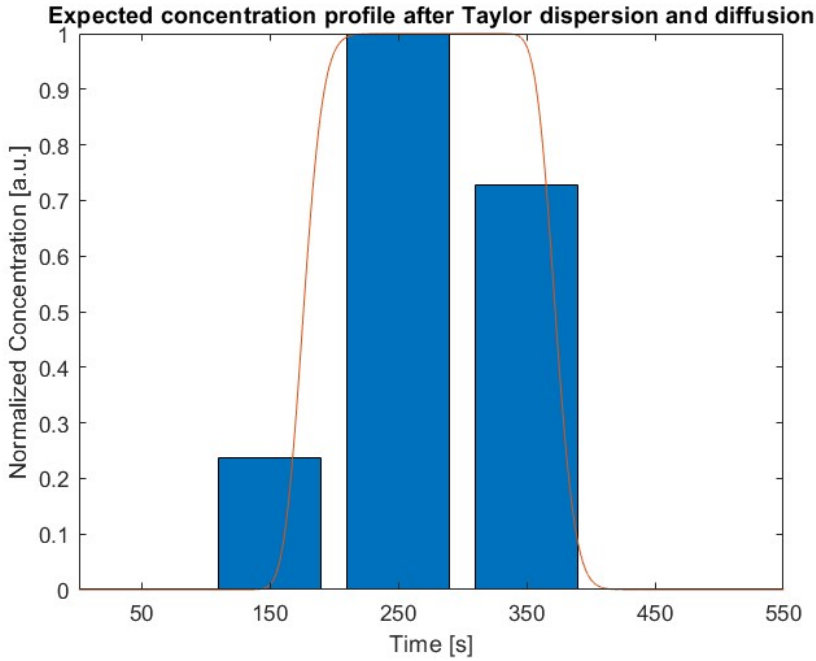

Figure 8: Expected sample dispersion with a smaller catheter outlet, at a flow rate $10nL/s$. The orange line shows the concentration profile over time, and the blue bars show how this profile would be distributed over plugs of $1\mu L$.

F.1 Sample Dispersion Script

```
clc
clear
close all;
%% Modelling the sample dispersion before the sample isolation stage
% In this model a combination of Taylor dipsersion and diffusion
% is modelled using impulse responses.



%% Variables
D = 2.84e-10; % Diffusion coefficient of Cortisol
Q = 2e-9/270; % Volumetric flow in cubic meters per second
period = 300; % time per sample
plug_volume = 1e-9; % Volume of the plug that will be created
flushed_volume = plug_volume*1; % volume to be flushed,
% set to 0 if no volume should be flushed
dt = 0.05; % Time step

%% constants

% Lengths
L_membrane = 10e-3;
L_outlet = 100e-3;
L_tubing = 10e-3;
L_channel = 5e-3;

% Diameters of cylindrical parts
d_membrane = 0.5e-3;
d_outlet = 0.38e-3;
d_tubing = 0.12e-3;

% Crossectional area of cylindrical parts
A_membrane = pi*(d_membrane/2)^2;
A_outlet = pi*(d_outlet/2)^2;
A_tubing = pi*(d_tubing/2)^2;

% Dimensions of the channel
h_channel = 189e-6;
w_channel = 756e-6;
r_channel = (h_channel^2 + 0.25*w_channel)/(2*h_channel);
theta_channel = 2*asin(0.5*w_channel/r_channel);
A_channel = 0.5*theta_channel*r_channel^2 - 0.5*w_channel*(r_channel-h_channel);

% Volumes
V_membrane = L_membrane*A_membrane;
V_outlet = L_outlet*A_outlet;
V_tubing = L_tubing*A_tubing;
V_channel = L_channel*A_channel;
V_sys = V_outlet + V_tubing + V_channel;

% flow speed
u_membrane = Q/A_membrane;
u_outlet = Q/A_outlet;
u_tubing = Q/A_tubing;
u_channel = Q/A_channel;

% Circumference
c_outlet = pi*d_outlet;
c_tubing = pi*d_tubing;
```

```
c_channel = w_channel + theta_channel*r_channel;

%% Determine Peclet numbers

% Peclet Numbers should be > 70
Pe_outlet = Q/(c_outlet*D);
Pe_tubing = Q/(c_tubing*D);
Pe_channel = Q/(c_channel*D);


%% Determine Reynolds numbers

% Reynolds numers should be < 2300
rho = 1e3;
mu = 1e-3;
Re_outlet = rho*mu*A_outlet/(c_outlet*u_outlet);
Re_tubing = rho*mu*A_tubing/(c_tubing*u_tubing);
Re_channel = rho*mu*A_channel/(c_channel*u_channel);

%% Determine Dispersion Coefficients
k_outlet = (d_outlet*u_outlet)^2/(4*48*D);
k_tubing = (d_tubing*u_tubing)^2/(4*48*D);
k_channel = (u_channel*2*A_channel/c_channel)^2/(48*D);

%% Time
% time needed to create one plug while the flow is on
plug_time = plug_volume/Q;

% Determine residence times
t_membrane = L_membrane/u_membrane;
t_outlet = L_outlet/u_outlet;
t_tubing = L_tubing/u_tubing;
t_channel = L_channel/u_channel;

% total average residence time of fluid
t_total = t_outlet + t_tubing + t_channel;

% Total time displayed on the x-axis
T = 3*dt*floor(t_total/dt);
% This value might need to be changed,
% if the total period is close to the inverse
% of the lowest frequencies that make up the signal.

% time array that will be used for the equations and plots
t = dt:dt:T;

%% Diffusion profiles
% Since the rest of the system is evaluated over time we need a base time
% array to be able to translate time to distance for the diffusion. It also
% has the same size as the original time array.
tau = -0.5*T:dt:0.5*T-dt;
t_diff = period - plug_time;

% Determine the impulse responses of the diffusion in each type of
% tubing/channel
Di_outlet = (1./sqrt(4.*pi.*D.*t_diff))*exp((-(tau.*u_outlet).^2)./(4*D*t_diff));
fft_Di_outlet = fft(Di_outlet);
Di_tubing = (1./sqrt(4.*pi.*D.*t_diff))*exp((-(tau.*u_tubing).^2)./(4*D*t_diff));
fft_Di_tubing = fft(Di_tubing);
Di_channel = (1./sqrt(4.*pi.*D.*t_diff))*exp((-(tau.*u_channel).^2)./(4*D*t_diff));
fft_Di_channel = fft(Di_channel);
```

```
%% Create begin pulse
t_pulse = floor(V_membrane/Q/dt)*dt;
pulse = zeros(1,length(t));
pulse(1:floor(t_pulse/dt)) = ones(1,floor(t_pulse/dt));

% Transform it to Fourier domain
fft_pulse = fft(pulse);

% create an object for the results
fft_res = fft_pulse;
%% Smearing effect of the catheter outlet
% determine how many full periods occur in the outlet
n_out = (t_outlet - mod(t_outlet, plug_time)) / plug_time;
t_out_rem =  mod(t_outlet, plug_time);

% apply the expected smearing in the outlet
if n_out > 0
    f_outlet = sqrt(plug_time./t).*exp(-(u_outlet.*t - L_outlet).^2./(4.*k_outlet.*t));
    fft_outlet = fft(f_outlet);
    for i=1:n_out
        fft_res = fft_res.*fft_outlet.*fft_Di_outlet;
    end
end

% apply the smearing of the partial period
f_outlet_rem = sqrt(t_out_rem./t).*exp(-(u_outlet.*t - L_outlet).^2./(4.*k_outlet.*t));
fft_outlet_rem = fft(f_outlet_rem);
fft_res = fft_res.*fft_outlet_rem;

%% Smearing effect of the tubing
% determine how much smearing effect the tubing has before the next pause
t_tub_pre = plug_time - t_out_rem;

% determine how the time spend in the tubing is spread out over periods
if t_tub_pre <= t_tubing
    n_tub = (t_tubing - t_tub_pre - mod(t_tubing - t_tub_pre, plug_time)) / plug_time;
    t_tub_rem =  mod(t_tubing - t_tub_pre, plug_time);

else
    n_tub = 0;
    t_tub_rem =  t_out_rem - t_tubing;
    t_tub_pre = t_tubing;
end

% apply the smearing effect before the pause
f_tubing_pre = sqrt(t_tub_pre./t).*exp(-(u_tubing.*t - L_tubing).^2./(4.*k_tubing.*t));
fft_tubing_pre = fft(f_tubing_pre);
fft_res = fft_res.*fft_tubing_pre.*fft_Di_tubing;

% apply the expected smearing in the tubing
if n_tub > 0
    f_tubing = sqrt(plug_time./t).*exp(-(u_tubing.*t - L_tubing).^2./(4.*k_tubing.*t));
    fft_tubing = fft(f_tubing);
    for i=1:n_tub
        fft_res = fft_res.*fft_tubing.*fft_Di_tubing;
    end
end

% apply the smearing of the partial period
```

```
f_tubing_rem = sqrt(t_tub_rem./t).*exp(-(u_tubing.*t - L_tubing).^2./(4.*k_tubing.*t));
fft_tubing_rem = fft(f_tubing_rem);
fft_res = fft_res.*fft_tubing_rem;

%% Smearing effect of the channel

% determine how much smearing effect the channel has before the next pause
t_cha_pre = plug_time - t_tub_rem;

% determine how the time spend in the tubing is spread out over periods
if t_cha_pre <= t_channel
    n_cha = (t_channel - t_cha_pre - mod(t_channel - t_cha_pre, plug_time)) / plug_time;
    t_cha_rem =  mod(t_channel - t_cha_pre, plug_time);
else
    n_cha = 0;
    t_cha_rem = t_tub_rem - t_channel;
    t_cha_pre = t_channel;
end

% apply the smearing effect before the pause
f_channel_pre = sqrt(t_cha_pre./t).*exp(-(u_channel.*t - L_channel).^2./(4.*k_channel.*t));
fft_channel_pre = fft(f_channel_pre);
fft_res = fft_res.*fft_channel_pre.*fft_Di_channel;

% apply the smearing expected in the channel
if n_cha > 0
    f_channel = sqrt(plug_time./t).*exp(-(u_channel.*t - L_channel).^2./(4.*k_channel.*t));
    fft_channel = fft(f_channel);
    for i=1:n_cha
        fft_res = fft_res.*fft_channel.*fft_Di_channel;
    end
end

% apply the remaining smearing expected in the channel
f_channel_rem = sqrt(t_cha_rem./t).*exp(-(u_channel.*t - L_channel).^2./(4.*k_channel.*t));
fft_channel_rem  = fft(f_channel_rem);
fft_res = fft_res.*fft_channel_rem;

n_total =  ceil(t_total / plug_time);

result = abs(ifft(fft_res));

%% Plots
figure
plot(t,pulse)
hold on
plot(t, sum(pulse)*result/sum(result))
title({"Expected sample dispersion due to Taylor dispersion",
       "including impulse responses of various subsections of the system"})
xlabel("Time [s]")
ylabel("Normalized Concentration [a.u.]")
legend("Pulse", "Result")
%% Expected plug concentration
% use a bar graph to combine the expected plug concentrations with the

% determine the number of data points per plug and create objects
ndt = plug_volume/(Q*dt);
res = zeros(1,floor(T/dt/ndt));
flushed = zeros(1,floor(T/dt/ndt));
t_ds = 0.5*plug_time:plug_time:T;
```

```
n_flush = flushed_volume/plug_volume;
cnt = n_flush;

% Loop over the expected plugs and determine their cortisol concentration
for i=1:floor(T/dt/ndt)
    if cnt == n_flush
        res(i) = mean(result(floor((i-1)*ndt+1):floor(i*ndt)));
        flushed(i) = 0;
        n_flush = 0;
    else
        res(i) = 0;
        flushed(i) = mean(result(floor((i-1)*ndt+1):floor(i*ndt)));
        n_flush = n_flush+1;
    end
end

% normalize the results back to the original total concentration
res_n = sum(pulse)*res/sum(result);
flushed_n = sum(pulse)*flushed/sum(result);

% Plot the results
figure
bar(t_ds(1:length(res_n)),res_n)
hold on
bar(t_ds(1:length(res_n)), flushed_n)
hold on
plot(t, sum(pulse)*result/sum(result))
title("Expected sample dispersion due to Taylor dispersion")
xlabel("Time [s]")
ylabel("Normalized Concentration [a.u.]")
xlim([1, t_ds(end)])
legend("Concentration in stored plug",
       "Concentration in flushed plug",
       "Concentration before plugs")
```

G Final Chip Fusion Files

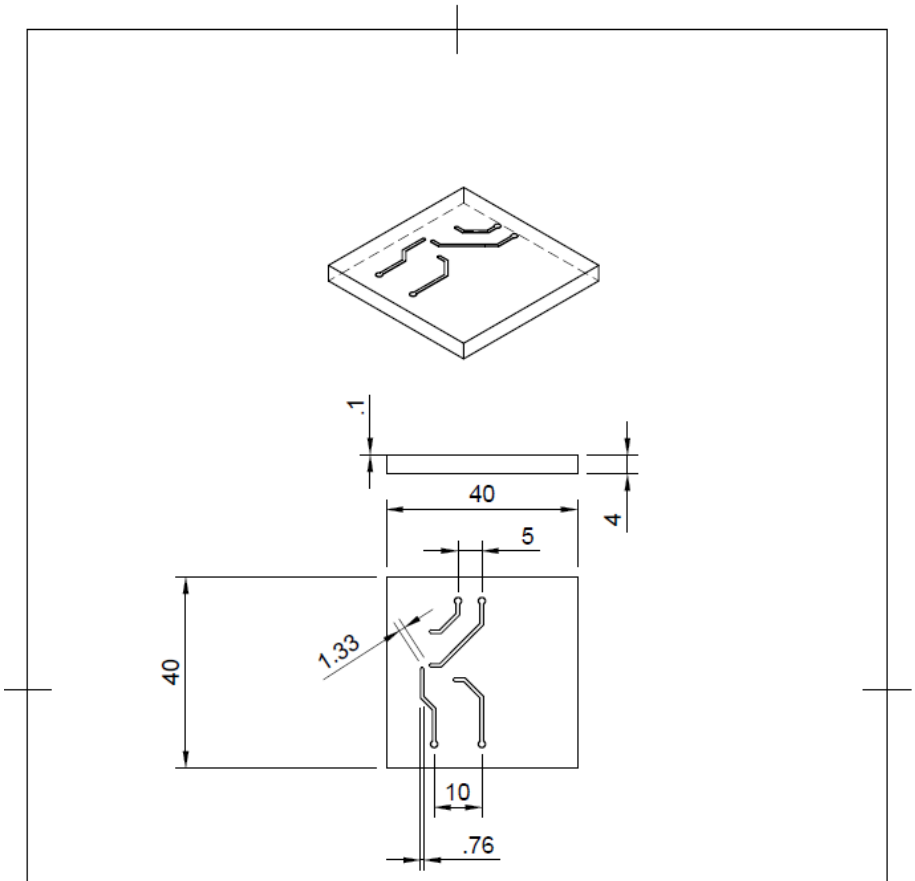

Dept.	Technical reference	Created by	Approved by
BIOS		Hidde Sikkema 22/06/2024	
All dimensions in the drawing are in mm.		Document type	Document status: Complete
		Title: Droplet Generator Control Layer	DWG No.
			Rev. / Date of issue / Sheet: 1/1

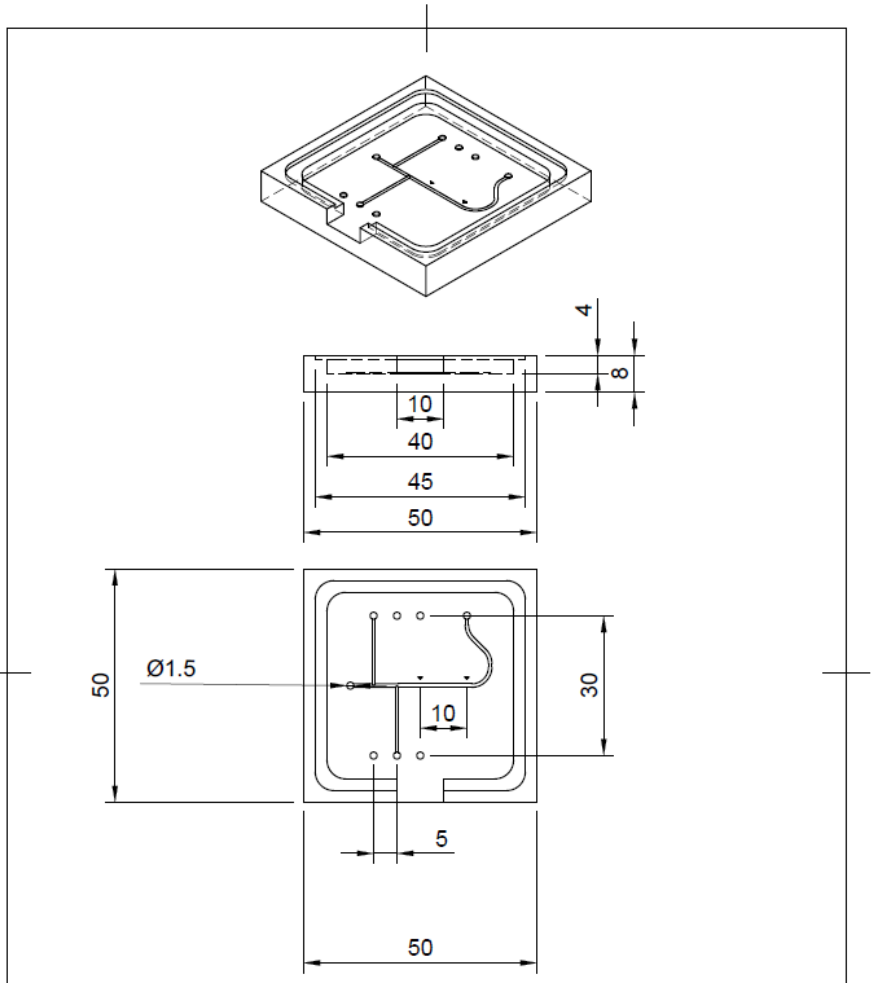

Dept.	Technical reference	Created by	Approved by
BIOS		Hidde Sikkema 22/06/2024	
All dimensions in the drawing are in mm.		Document type	Document status: Complete
		Title: Droplet Generator Flow Layer	DWG No.
			Rev. / Date of issue / Sheet: 1/1